

December 2011

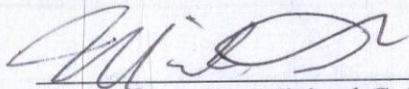
CHARACTERIZING EKLUTNA GLACIER'S RESPONSE TO CLIMATE THROUGH
MEASUREMENTS OF MASS BALANCE, GEOMETRY, AND MOTION

written by

Louis C. Sass

THESIS

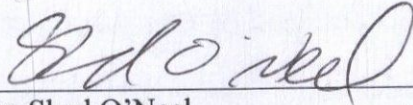
APPROVED: Thesis Committee



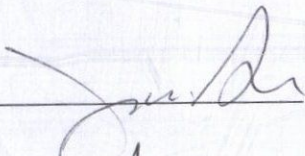
Chairperson: Dr. Michael G. Loso

12/15/11

Date

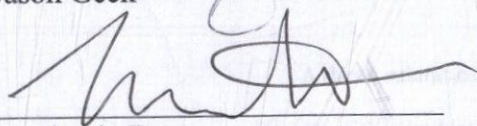


Dr. Shad O'Neel



Jason Geck

ACCEPTED:



Academic Dean

12/13/11

Date

Characterizing Eklutna Glacier's Response to Climate Through
Measurements of Mass Balance, Geometry, and Motion

by

Louis C. Sass

A thesis submitted to the
Faculty of the Graduate School of
Alaska Pacific University
In partial fulfillment
Of the requirement for the degree
Master of Science
Department of Environmental Science

2011

Abstract

This work examines enhanced thinning in and near the accumulation zone on the main branch of Eklutna Glacier, Alaska. I first present measurements of surface mass balance and surface elevation to document the enhanced thinning and understand the implications for stability in the present climate. I then present radar and GPS surveys to characterize the associated dynamics. Measurements of surface mass balance from 2008–10 and surface elevations in 1957, 2007, and 2010, show that thinning in the upper basin is shifting the area altitude distribution to lower elevation, and forcing future mass balance to be more negative in a given climate. This suggests future mass loss will increase even without further climate forcing. Radar profiles show the broad, flat, upper basin to be overdeepened, and separated from the lower glacier by a shallow riegel. Surface velocities increase through this constriction. We used a force balance and partition the resistive stresses into components. The longitudinal drag term accentuates the variations in driving stress, indicating that the velocities are largely governed by the large changes in ice thickness and cross sectional area. Combined longitudinal and lateral drags presently resist half of the driving stress in the upper basin, so understanding how these vary in time will be critical for future glacier geometry and mass balance.

Table of Contents

Chapter 1: Surface mass balance and enhanced thinning of the accumulation zone at Eklutna Glacier, Alaska.....		1
1.1. INTRODUCTION.....		2
1.1.1. Setting.....		3
1.2. DATA.....		7
1.2.1. Mass Balance.....		7
1.2.2. Surface Elevation Change.....		8
1.3. ANALYSIS AND RESULTS.....		10
1.3.1. Mass Balance.....		10
1.3.2. Surface Elevation Change.....		14
1.4. Uncertainties.....		20
1.5. Comparison of Methods.....		22
1.6. DISCUSSION.....		23
1.6.1. Area Altitude Distribution Change.....		23
1.6.2. Long-Term Trends in Mass Balance.....		26
1.6.3. Continuity and Ice Flux.....		27
1.6.4. Broader Implications.....		31
1.7. SUMMARY.....		31

Chapter 2: Ice geometry and motion associated with enhanced thinning in the accumulation zone of Eklutna Glacier, Alaska.....	39
2.1. INTRODUCTION.....	40
2.1.1. Setting.....	42
2.2. METHODS.....	43
2.2.1. Data Collection.....	44
2.2.2. Analysis.....	45
2.3. RESULTS.....	51
2.4. UNCERTAINTIES.....	55
2.5. DISCUSSION.....	58
2.5.1. Geometric Control of the Flow-Field.....	58
2.5.2. Force Balance.....	59
2.5.3. Implications.....	60
2.6. CONCLUSIONS.....	61
Data CD contents.....	67

List of Figures

Figure 1.1: Eklutna Glacier overview.....	4
Figure 1.2: Mass balance sites and laser altimetry profiles.....	5
Figure 1.3: Profile comparison of LiDAR, laser altimetry, and SPOT DEM.....	9
Figure 1.4: Balance profiles and AADs.....	12
Figure 1.5: Mass Balance Maps.....	13
Figure 1.6: 1957–2010 Annual surface elevation change.....	15
Figure 1.7: Raw difference between laser altimetry to LiDAR.....	16
Figure 1.8: Ablation season 2007 correction terms.....	17
Figure 1.9: 2007–2010 Annual surface elevation change.....	19
Figure 1.10: Change in area-altitude distribution.....	24
Figure 1.11: Mass balance comparison with Wolverine Glacier.....	27
Figure 1.12: 2008–2010 ice flux calculated from mass continuity.....	29
Figure 2.1: 2009 Radar transects and survey network.....	43
Figure 2.2: Measured ice thickness.....	50
Figure 2.3: Bed elevations.....	50

Figure 2.4: Surface velocities.....51

Figure 2.5: Ice-flux comparison and depth averaged velocity correction.....52

Figure 2.6: Centerline velocities and normal strain rates.....53

Figure 2.7: Force balance terms.....54

Appendix 2.1: Summer LPI surface velocities.....62

Preface

List of Tables

Table 1.1: Glacier wide surface mass balance and ELAs, 2008–10.....	10
Table 1.2: Change in surface elevation vs change in surface mass balance.....	22
Appendix 1.1: Mass balance measurements.....	36
Appendix 2.1: Summer 2009 surface velocities.....	66

Preface

The format of this thesis is two separate chapters. The first chapter documents surface mass balance and enhanced thinning in the accumulation zone to analyze the stability of Eklutna Glacier in the present climate. The second chapter uses radar and GPS surveys to characterize the dynamics associated with the enhanced accumulation zone thinning. Each chapter is intended to be submitted as a separate paper to *Journal of Glaciology*. Chapter 1 has gone through a number of revisions and all of the co-authors have had opportunity to comment on all sections. It is very close to the product that will be submitted soon. Chapter 2 is a much less polished product. None of the co-authors have commented on the current discussion, and it could change in substantial ways.

Chapter 1: Surface mass balance and enhanced thinning of the accumulation zone at Eklutna Glacier, Alaska

Louis C. Sass,^{1,2} Michael G. Loso,¹ Shad O'Neel,² Christopher F. Larsen³

¹*Alaska Pacific University, 4101 University Dr, Anchorage, AK, 99508, USA*

²*United States Geological Survey Alaska Science Center, 4230 University Dr, Anchorage, AK, 99508, USA*

³*Geophysical Institute, University of Alaska Fairbanks, 903 Koyukuk Dr, Fairbanks, AK, 99757, USA*

ABSTRACT. We examine the enhanced thinning of the accumulation zone, and the resulting implications for stability, at Eklutna Glacier, Alaska. This glacier is 30 km², land terminating, and shows no signs of surge activity, yet the thinning in the accumulation zone is shifting the area altitude distribution lower and forcing surface mass balance to more negative values. We document these effects with direct measurements of surface mass balance in 2008–10 and surface elevation changes between 1957, 2007, and 2010. Glacier wide mass balance values for 2008–10 with direct methods agree with geodetic methods and are -1.3 ± 0.3 m (ice equivalent). The 2008–10 balance flux fails to make it out of the upper basin, so ice flux to the entire lower half of the glacier is supported solely through thinning. This is especially significant as comparison with the >40 year mass balance record on nearby Wolverine Glacier suggests 2008–10 is a positive anomaly in the mass balance of the previous 20 years and similar to the long-

term average. Continued thinning in and near the accumulation zone is in a positive feedback with surface mass balance, and the present glacier geometry is not stable in the present climate.

1.1. INTRODUCTION

Accumulation zone profiles of mountain glaciers are generally thought to be relatively insensitive to changes in climate (e.g., Nye, 1960; Holmlund, 1988; Johannesson and others, 1989, Schwitter and Raymond, 1993). This stability arises from the non-linear rheology of ice deformation (Glen, 1952), and the predominance of simple shear (Nye, 1952), allowing large changes in ice flux to be accommodated with minimal changes in ice thickness (e.g., Hutter, 1981). Hence the geometric changes associated with a stable response to a perturbation in climate occur primarily at the terminus, with advance or retreat altering the glacier geometry so that glacier-wide mass balance shifts back toward the equilibrium value of 0 (Nye, 1960).

The unstable response to a perturbation in climate occurs when the geometric changes force the glacier-wide mass balance further away from equilibrium. The classic B \ddot{o} varsson (1955) instability arises from a positive feedback between changes in surface elevation and changes in surface mass balance. If a glacier is sufficiently flat, and the balance profile is a typical monotonically increasing function of surface elevation, then a reduction in the surface mass balance rate will decrease the ice flux, which in turn decreases the ice thickness, and reduces the surface mass balance even further

(Böðvarsson, 1955; Nye, 1960; Weertman, 1961; etc.). For this feedback to actually cause an instability the glacier bed needs to be nearly flat or even reverse, as is the case on some ice sheets and ice caps, but not generally on mountain glaciers. More recently Harrison and others (2001) reiterated the destabilizing effect of changes in ice thickness to glacier mass balance in general, albeit with analysis limited to glacier wide averages. Thus it is important to quantify present rates of change in the accumulation zone and the resultant mass balance forcing in order to understand potential future impacts of these effects.

1.1.1. Setting

Eklutna Glacier is a small (10.4 km long, 29.7 km² in area) mountain glacier in southcentral Alaska's Chugach Mountains (Figure 1.1). Runoff from the glacier flows into Eklutna Reservoir, which provides ~80% of municipal water and 10–20% of the total municipal electrical power (Moran and Galloway, 2006) to Anchorage, Alaska's largest city. Despite the fact that the glacier covers <10% of the reservoir catchment area, 45–50% of the total reservoir inflow is runoff from the glacier (Larquier, 2011). Thus there is a need for a comprehensive understanding of the glacier mass budget and its response to climate change.

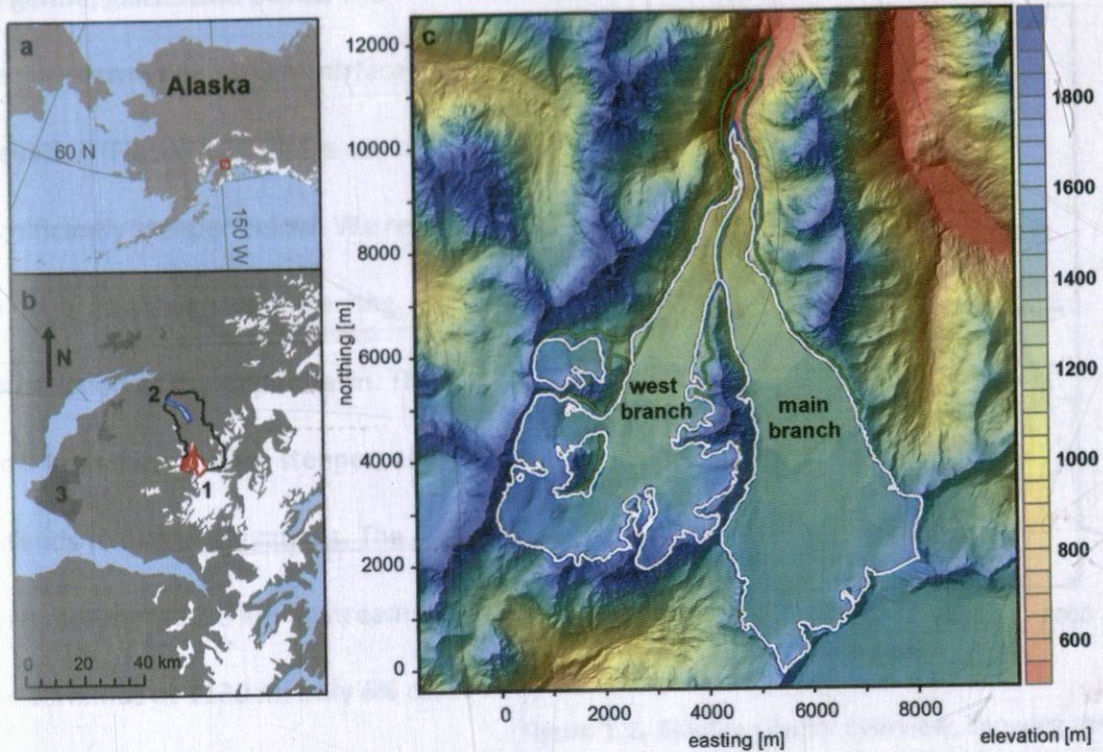


Figure 1.1. Eklutna Glacier is located in southcentral Alaska (a). Runoff from the glacier (b 1) is the principal component in the annual water budget of the Eklutna Reservoir (b 2) despite covering <10% of the basin area (black polygon). The reservoir is used for drinking water and hydropower for Anchorage (b 3). Eklutna Glacier topography (c) from 16 September, 2010 LiDAR. Two branches (the main branch on the right and the west branch on the left) flow together to form one terminus. Glacier outlines for 1957 (green – from U.S. Geological survey 1:63,600 map), 2007 (blue – from 2007 SPOT 5), and 2010 (white – from 2010 LiDAR) show 1.8 km of terminus retreat, however the change in area from terminus retreat is less than 5%. In c the minimum easting and northing are subtracted from the Universal Transverse Mercator (UTM) coordinate system (zone 6N, WGS84) for simplification ($x = \text{UTM}_E - 388812$; $y = \text{UTM}_N - 6783612$).

The glacier proper flows from 2100 m elevation summits down to its present 520 m elevation terminus. Two branches converge below the equilibrium line altitude (ELA), which we refer to as the main branch (56% of the area) and the west branch (44% of the area). The main branch is characterized by a broad, flat upper basin that is surrounded

by gentle, glacierized peaks. The glacier narrows at 1360 m surface elevation (Figure 1.2), and is significantly steeper below. We refer to the area above this narrowing constriction as the upper basin. The west branch is smaller, steeper, and extends to higher elevations. The branches merge 2.9 km upstream of the terminus at 1130 m; only 6% of the total area is found below the convergence. A medial moraine delineates the contributions of each branch, and the west branch terminates 0.5 km above the main branch.

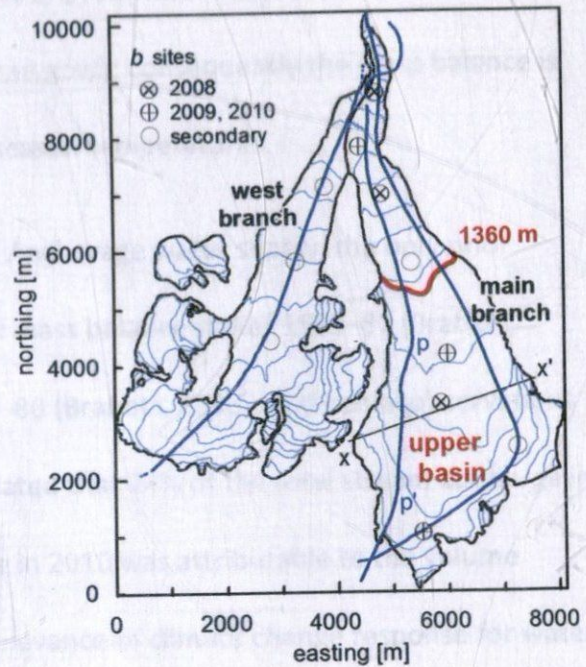


Figure 1.2. Eklutna Glacier overview, showing the mass balance sites used each year and the May 6 2007 laser altimetry profiles (dark blue lines). We refer to the area above 1360 m in the main branch (red line) as the upper basin. The cross-flow and along-flow profiles x to x' and p to p' are shown in figure 1.3.

Eklutna Glacier is located 50 km northwest of Alaska's Prince William Sound and the Gulf of Alaska in a transitional climate between maritime and continental regimes. Mass turnover rates (Meier and others, 2003) are high, from 3–5 m w.e. a^{-1} . A 4–6 m snow-pack is typical in the accumulation area (roughly >1450 m elevation) by the end of winter. Ablation rates at the terminus range from -8–10 m a^{-1} . Temperatures near the ELA vary from lows below -30° C in winter to highs above 10° C in summer. Although

interannual variability is significant, 50–60% of precipitation falls in the four months from July to October (<http://www.ncdc.noaa.gov/>); consequently the mass balance is sensitive to small differences in shoulder season temperatures.

Despite the relevance of the glacier to Anchorage water supply, the only prior research consists of incomplete surveys of mass balance stakes 1985–87 (Brabets, 1993), stream gauge measurements 1985–88 (Brabets, 1993), and casual observations of terminus retreat. Larquier (2011) estimated that 24% of the total stream discharge in 2009 and 3% of the total stream discharge in 2010 was attributable to the volume change on the glacier, underscoring the relevance of climate change response for water resources.

In this paper we present surface mass balance (2008–10) and surface elevation data (1957, 2007, and 2010) from Eklutna Glacier to demonstrate that accumulation zone thinning is occurring and that it represents an unstable response to ongoing climatic changes. We compare volume changes calculated from direct surface mass balance measurements to those estimated from measured surface elevation change. We show that widespread thinning of the accumulation zone is ongoing, and that the bulk of the area altitude distribution (AAD) is shifting to lower elevation. This shift in the AAD will force future mass balance to be more negative in a given climate. Comparison of the relative roles of surface mass balance and thickness changes show that the 2008–10 ice-

flux was largely supported by thickness changes on the upper glacier, and the surface mass balance would support a glacier less than half the present length.

1.2. DATA

Two types of data form the basis of our analysis of Eklutna Glacier: direct observation of surface mass balance and remotely-sensed measurements of surface elevation change.

An overview of Eklutna Glacier and the data are shown in Figure 2. The minimum easting and northing are subtracted from the Universal Transverse Mercator (UTM) coordinate system (zone 6N, WGS84) for simplification ($x = \text{UTM}_E - 388812$; $y = \text{UTM}_N - 6783612$).

1.2.1. Mass Balance

We measured surface mass balance (b_{sfc}) with standard glaciological methods (Hubbard and Glasser, 2005) on a seasonal basis from 2008–2010. Stake and pit measurements in spring and fall document accumulation (c_{sfc}) and ablation (a_{sfc}) at three sites carefully chosen to be representative of broad regions and located near the centerline of the main branch (Figure 1.2). In 2009–10, sites were re-located to better distribute them over the area altitude distribution (AAD) and we documented the position of the ELA. Observations made at up to five secondary sites compliment the measurements at the three main sites. Secondary sites generally lack density measurements, but are useful in constraining extrapolation techniques. We maintained

an on glacier weather station near the ELA each ablation season, with measurements of temperature, precipitation, ablation rates (via sonic range finder), wind speed and direction, and albedo (with upward and downward facing pyranometers).

No attempt was made to estimate internal or basal processes; herein "mass balance" refers only to the "surface mass balance" of Cogley and others (2011). We measured stake position by collecting single frequency GPS data and post-processed against continuously operating reference stations (CORS) located within 40 km of the glacier.

1.2.2. Glacier Surface Elevation Change

Glacier surface elevation changes are obtained from analysis of three independent surface elevation measurement campaigns that occurred during 1957, 2007, and 2010. We refer to each data set by the year of collection.

Digital Elevation Models (DEMs) produced from 12 July, 1957 imagery, and contained in the U.S. Geological Survey National Elevation Dataset (NED; Gesch and others, 2002) provide baseline data for our analysis. The 2 arc-second ($\sim 30 \times 60$ m) DEMs are derived from 1:63,360 maps with a 100 ft (~ 30 m) contour interval and a stated vertical accuracy of 50 ft (~ 15 m). Previous research has concluded that errors in accumulation zone areas can exceed the stated accuracy (Echelmeyer and others, 1996; Aðalgeirsdóttir and others, 1998). We assume an uncertainty of ± 45 m in snow-covered

areas (Arendt and others, 2002), which were identified via inspection of the original photography.

The University of Alaska Fairbanks acquired three airborne laser altimetry profiles on 6 May 2007 (Figure 1.2), including one profile along the centerline of the west branch, and two profiles spaced out in the broader main branch. The system achieves horizontal point spacing of 1.5 m with a vertical accuracy ~ 0.3 m (Echelmeyer and others, 1996; Arendt and others, 2002). We also used a 16 July, 2007 ortho-rectified SPOT 5 image (Korona and others, 2009) to determine the 2007 glacier area, but did not use the associated DEM, due to evidence of errors exceeding 10 m in the accumulation zone (Figure 1.3).

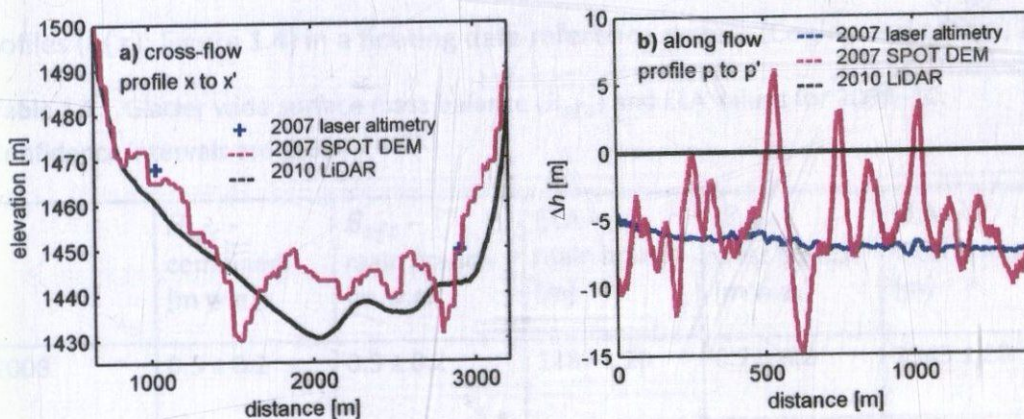


Figure 1.3. a) Cross section (from x to x' in figure 2) showing the 2010 LiDAR surface (black), the 2007 laser altimetry profiles (blue) and the SPOT 5 DEM (pink). Note the 30x vertical scale exaggeration. b) change in ice thickness (Δh) from the 2010 LiDAR along a laser altimetry profile in the upper basin of the main branch (from p to p' in figure 1.2). As the local variance in the SPOT 5 DEM is larger than the total magnitude of change in ice thickness, we excluded the SPOT based elevations from our analysis.

Finally, we obtained a DEM resulting from an airborne LiDAR mission, flown on 16 September 2010, that covered the entire glacier (Figures 1.1, 1.2). It was collected with an Optech Gemini Airborne scanning system and resulted in a point cloud with nominal point density of 1.9 m and a reported vertical accuracy of 0.3 m. The U.S. Geological Survey EROS data center processed the point cloud data by filtering outliers and used a triangulated irregular network to create a 2.5 m DEM (<http://lidar.cr.usgs.gov/>).

1.3. ANALYSIS AND RESULTS

1.3.1. Mass Balance

Point measurements allowed construction of piecewise linear annual surface balance profiles ($b(z)$; Figure 1.4) in a floating date reference system (Cogley and others, 2011;

Table 1.1. Glacier wide surface mass balance (B_{sfc}) and ELA values for 2008–10. Confidence intervals are 95%

	B_{sfc} - combined [m w.e.]	B_{sfc} - main branch [m w.e.]	ELA - main branch [m]	B_{sfc} - west branch [m w.e.]	ELA - west branch [m]
2008	0.5 ± 0.2	0.5 ± 0.2	1287 ± 20	0.7 ± 0.2	1343 ± 20
2009	-1.5 ± 0.2	-1.7 ± 0.2	1532 ± 5	-1.2 ± 0.2	1620 ± 12
2010	-0.2 ± 0.2	-0.2 ± 0.2	1399 ± 5	-0.3 ± 0.2	1495 ± 17
Cumulative 2008-10	-1.2 ± 0.3	-1.4 ± 0.2	1460 ± 8	-0.8 ± 0.3	1512 ± 15

Appendix 1.1.). Glacier-wide surface mass balance varied from $+0.5 \pm 0.2$ m w.e. to -1.5 ± 0.2 m w.e. and the cumulative mass balance 2008–10 is -1.2 ± 0.3 m w.e. (Table 1.1). The three years of observation include positive and negative balances as well as an anomaly. The details of our analysis follow.

We calculated an average ELA for each branch by locating the end of season firn line on the DEM surface from oblique aerial photography. The ELA was consistently higher in the west branch, in accordance with observations of significantly lower accumulation and slightly lower ablation. The differences in surrounding topography likely influence the surface mass balance in substantially different ways, which prompted us to calculate separate balance profiles for each branch (Figure 1.4). For the west branch, where observations are sparse, we assume a linear balance profile between the confluence and the ELA.

Integration of each balance profile over the branch surface yielded the balance for each branch individually. An area weighted average then gave the glacier-wide mass balance (B_{sfc}) (Figure 1.5). Glacier area changes were obtained by linear interpolation between the 2007 and 2010 glacier outlines, but all glacier-wide balances were derived by integration over the 2010 DEM at 10 m resolution. The effect of the change in surface elevation for 2008–09 was approximated by using the 2010 DEM surface elevation associated with the horizontal coordinate of the 2008–09 mass balance sites.

A mass balance anomaly exists for 2009 as a result of a volcanic eruption at nearby Mt. Redoubt that deposited $\sim 90 \text{ g/m}^2$ of tephra on the glacier surface during March (Schaffer, 2011). The tephra caused a $\sim 25\%$ decrease to surface albedo as compared to 2008 and 2010. Coupled with warmer than average temperatures, reduced albedo enhanced ablation and exposed a broad swath of the 1992 Crater Peak Tephra (Neal

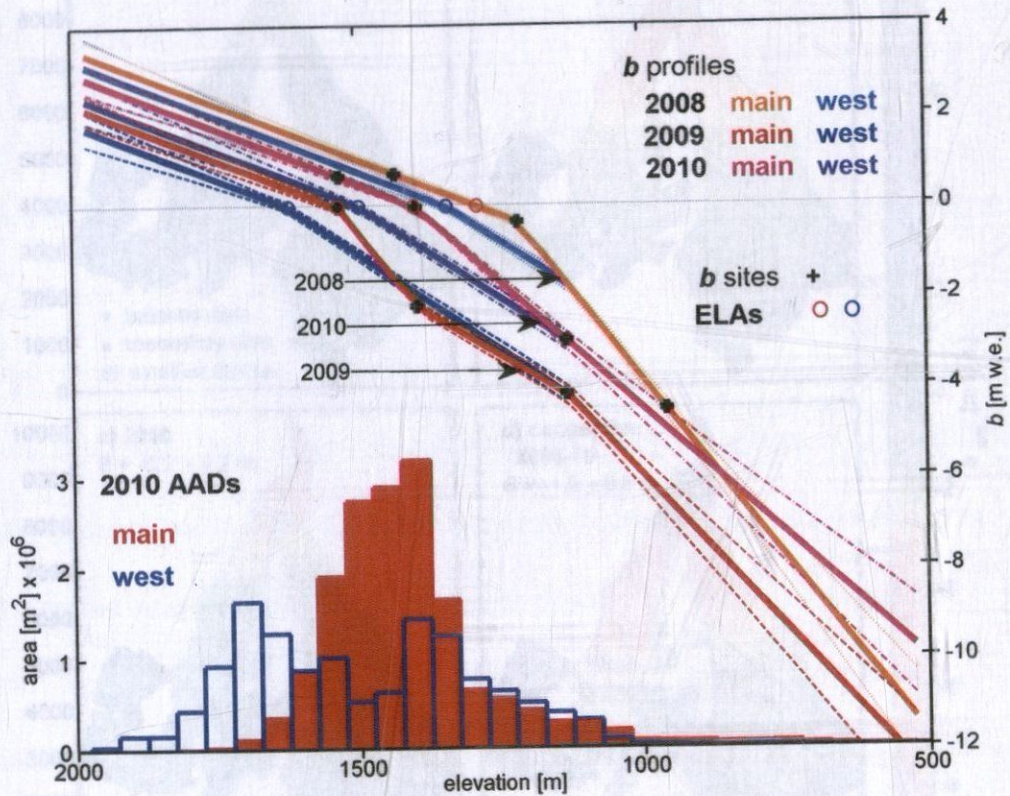


Figure 1.4. Eklutna Glacier surface mass balance data and extrapolated profiles for 2008–10 are shown on the right axis. The main branch is shown in the red tones; the west branch is shown in the blue tones. Confidence intervals are the thin lines. The kink in the main branch 2009 balance profile was caused by a significant reduction in albedo associated with a broad band of the 1992 Crater Peak Tephra exposed at the surface between 1370 and 1415 m. The area altitude distributions (50 m bin size) of the two branches are shown on the left axis.

and others, 1995) near and below the middle site. This exposed tephra further lowered the surface albedo, resulting in a more negative balance at the middle site. Rather than a linear extrapolation outside of the range of sites, we matched the profile slopes to the 2008 and 2010 profiles.

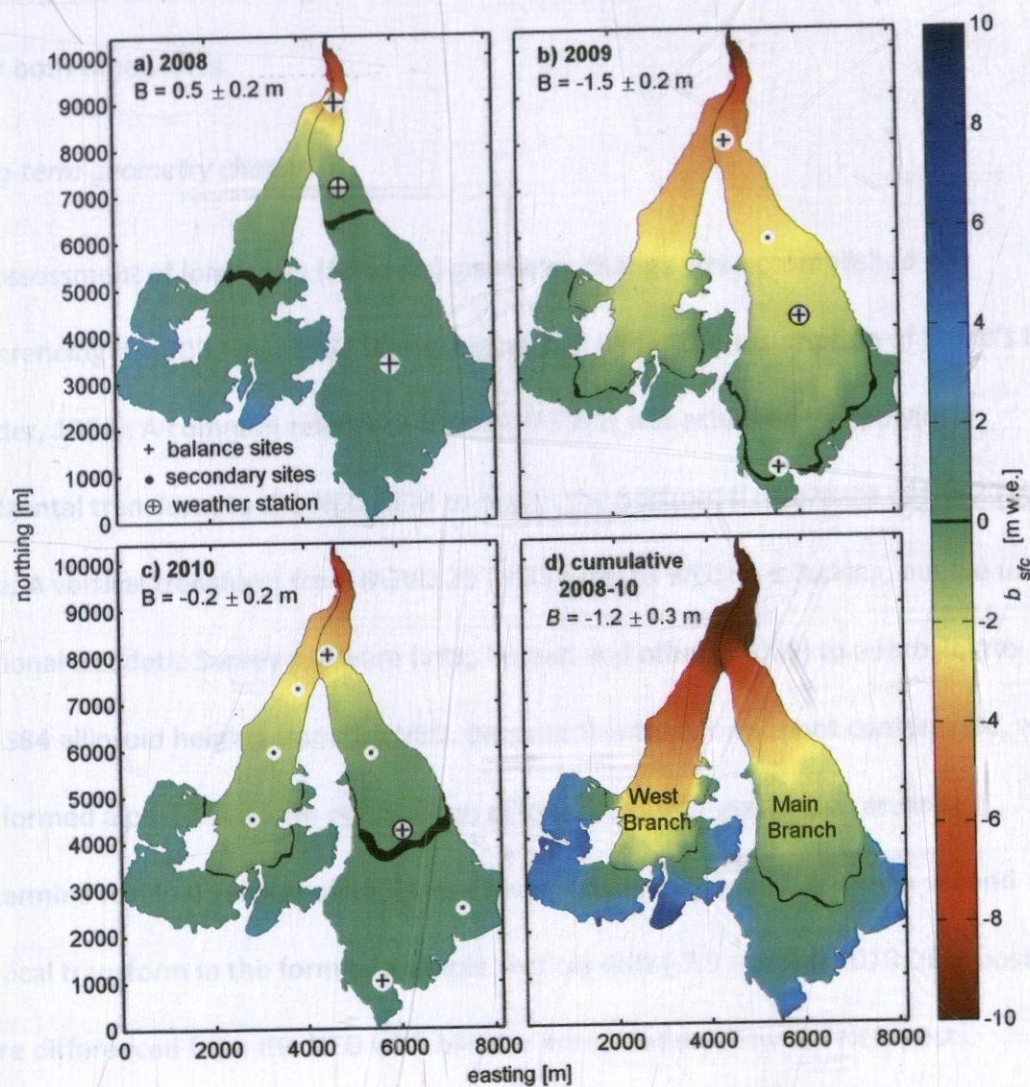


Figure 1.5. Mass balance results, 2008–10, m w.e. Mass balance profiles from Figure 4 extrapolated by elevation. Black represents neutral balance and the ELA. See appendix 1.1. for accumulation (c_{sfc}), ablation (a_{sfc}), and balance (b_{sfc}), at each of the primary sites. See table 1.1 for ELA elevations of each branch.

1.3.2. Glacier Surface Elevation Change

We present surface elevation and volume change through analysis of the three surface elevation datasets. Spatial and temporal properties of each data set complicates both the long- and short-term calculations, but we show that consistent patterns emerge over both time scales.

Long-term geometry change

An assessment of long-term (53 years) geometry change was accomplished by differencing the 2010 and 1957 DEMs (Figure 1.6) under the assumption of Sorge's law (Bader, 1954). A common reference frame (WGS84) was achieved by applying a horizontal transform to the NED DEM to match the horizontal reference of the 2010 data. A vertical transform from NGVD 29 (NED data) to WGS84 is lacking, but we used National Geodetic Survey software (intg; Roman and others, 2009) to approximate WGS84 ellipsoid heights from the NED. Because this transform is not constrained, we performed a post-transform comparison of low slope, non-glacierized areas to determine residual vertical offset (Arendt and others, 2002), and applied a second vertical transform in the form of a simple vertical shift (-7.9 m). The 2010 DEM posts were differenced from the NED with bilinear interpolation between NED posts.

The total volume change (of undifferentiated snow and ice) on Eklutna Glacier from 1957–2010 was -1.2 km^3 . Normalization by the average glacier area gives a specific thickness change of $-41 \pm 33 \text{ m}$. The maximum surface elevation change was $-220 \pm 16 \text{ m}$

at the 2010 terminus. Below the upper basin, surface elevation changes decreased with elevation to the minimum change of -27 ± 17 m at 1300 m in the constriction. In the upper basin, however, surface elevation change increased to -76 ± 46 m at 1440 m (2010 surface). The mean specific annual rate of surface elevation change was -0.8 ± 0.6 m a⁻¹ (Figure 6). However, in the upper basin near the 1440 m contour mean surface elevation change was -1.4 ± 0.9 m a⁻¹.

Short-term geometry changes

Acquisition timing and the two-dimensional nature of the 2007 profile data complicated estimates of surface elevation change over the 2007–2010 interval. Differencing over short duration required accounting for seasonal thickness variations caused by surface mass balance and the vertical component of ice-flow. We partitioned the mass balance and ice-flow separately into components representing the 2007 ablation season and the

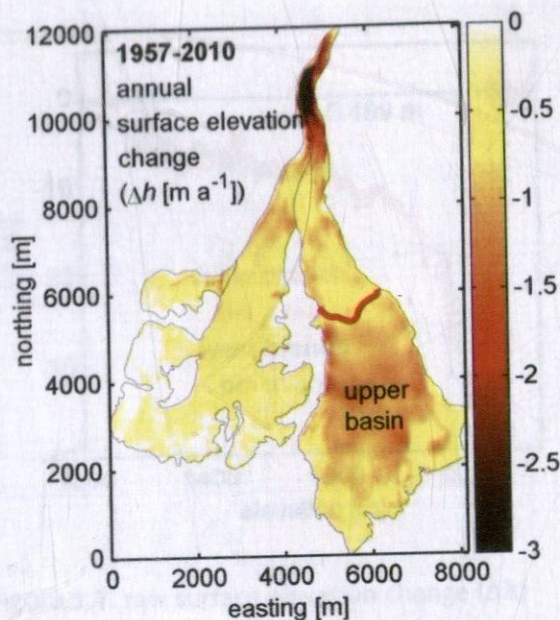


Figure 1.6. Surface elevation change for 1957–2010 normalized per year. 1360 m contour (2010) in the main branch shown in red. The upper basin of the main branch (>1360 m) shows more surface elevation change than the area just below 1360 m.

remainder of the interval, allowing us to estimate thinning between mass minima. This process entailed six steps.

1. *Datum Adjustment:* In a similar manner as described above, we rectified any differences in the vertical reference frame between the two data sets by comparing elevations over low-angle, non-glacierized, regions and adjusting as described in Appendix 2 (-0.50 m).

2. *Differencing:* Each 2007 elevation measurement was differenced from the 2.5 m 2010 DEM with a bilinear interpolation between DEM posts. Manual filtering was used to remove points on the lower glacier where large off-nadir topography caused reduced coherence.
3. *Construction of dz/z :* The 2010 topography was used to establish 50 m bins spanning the glacier's elevation range. Separate bins were established for each branch of the glacier. Within each bin, we calculated the mean surface elevation, and the mean surface elevation change (Figure 1.7). We fit a piece-wise linear

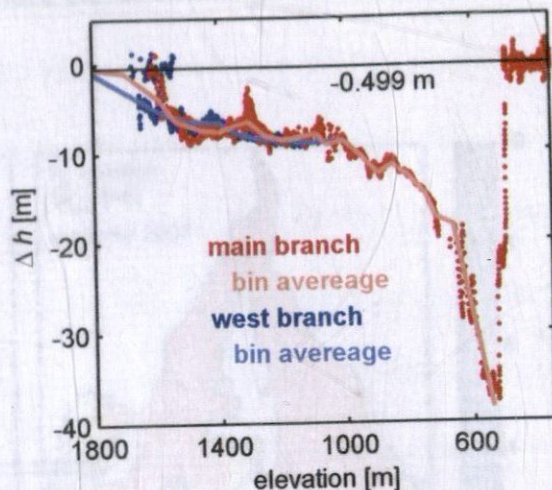


Figure 1.7. raw surface elevation change (Δh) between the May 6, 2007 laser altimetry and the September 16, 2010 LiDAR in the main branch (red) and the west branch (blue). The -0.499 m datum adjustment is shown in black. The 50 m bin average is shown with the lighter lines. Δh in the main branch becomes more negative above 1360 m. Note that we extrapolated from the highest on-glacier elevations under the laser altimetry profiles to the top of the area altitude distribution within each branch.

function and used this to calculate surface elevation change at each node in the 2010 DEM (Figure 1.8a).

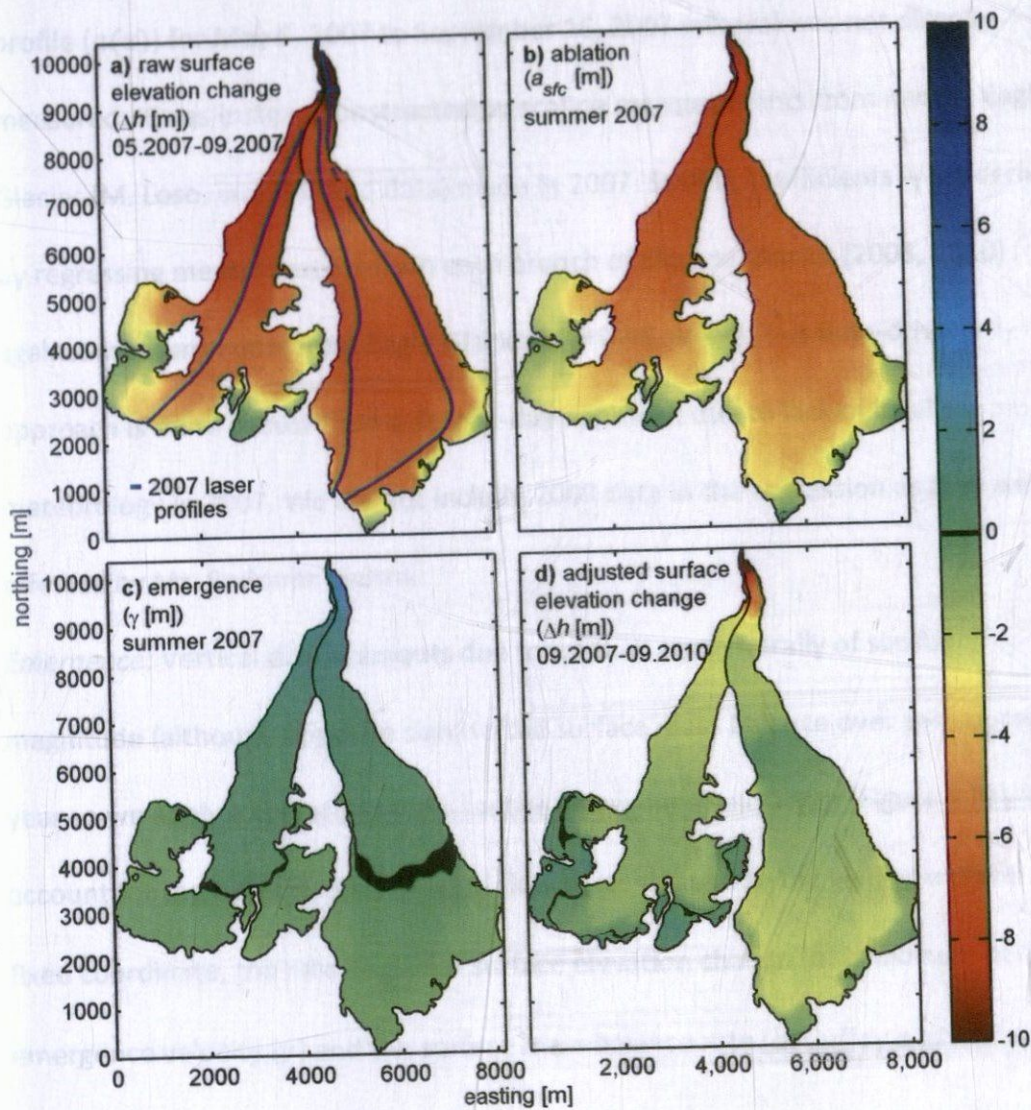


Figure 1.8. (a) Changes in surface elevation (Δh) calculated from the difference between 6 May, 2007 airborne laser altimetry (blue lines) and 16 September, 2010 LiDAR is extrapolated within each branch by elevation. A -0.499 m datum adjustment is included here based on off glacier points. (b) Meters of surface change from ablation summer 2007, modeled from nearby Eagle Glacier. (c) Elapsed emergence (γ) summer 2007. (d) Adjusted thinning map ($\Delta h - b_{07} + \gamma_{07}$ or $a-b+c$) representing surface elevation change from September 2007 to September 2010 and equivalent to the b years 2008–10.

4. *Ablation*: In a similar fashion as for the total surface elevation change, we assigned a 2007 ablation value to each node of the 2010 surface (Figure 1.8b). The ablation profile ($a(z)$) for May 6, 2007 to September 16, 2007 interval was not directly measured. It was instead constructed by scaling measurements from nearby Eagle Glacier (M. Loso, unpublished data) made in 2007. Scaling coefficients were derived by regressing measurements from each branch of Eklutna Glacier (2008, 2010) against measurements from Eagle Glacier ($r^2 = 0.98$, $n = 6$). This data-driven approach is more robust than a degree-day approach due to lack of local meteorology in 2007. We did not include 2009 data in the regression as they were affected by Mt. Redoubt tephra.
5. *Emergence*: Vertical displacements due to ice flow are generally of similar magnitude (although opposite sign) to the surface mass balance over the course of a year so we apply a correction term for the emergence velocity, γ (Figure 1.8c), to account for the upward or downward flow of ice relative to the glacier surface. At a fixed coordinate, the rate of glacier surface elevation change (\dot{h}) is the sum of the emergence velocity (γ) and the surface mass balance rate (\dot{b} ; Cuffey and Patterson, 2010), which can be rearranged to

$$\gamma = \dot{h} - \dot{b}. \quad (1)$$

We calculated the total emergence (Γ , also as a function of elevation) as the difference between the unadjusted total surface elevations change (step 2) and the cumulative surface mass balance over the interval (6 May 2007 – 16 Sept. 2010).

Because horizontal flow exhibits seasonal variability, this multi-annual average may not be a valid approximation for ablation-season emergence. Assuming that horizontal and vertical motion co-vary over broad regions, we estimated the ratio of summer to annual motion as a function of elevation to allow the resolution of both summer and winter emergence rates as a function of elevation. From mass continuity glacier-wide emergence must sum to zero. We found our estimate fulfilled this requirement in the main branch but deviated from this requirement in the west branch. We adjusted the emergence profile within the west branch with a vertical shift of -0.03 m a^{-1} to conserve mass.

6. *Adjusting for seasonal variability:* Both ablation (step 4) and emergence (step 5) were subtracted from the estimate of total surface elevation change to give the seasonally adjusted surface elevation change (Figure 1.8d) representing the time period 16 September, 2007

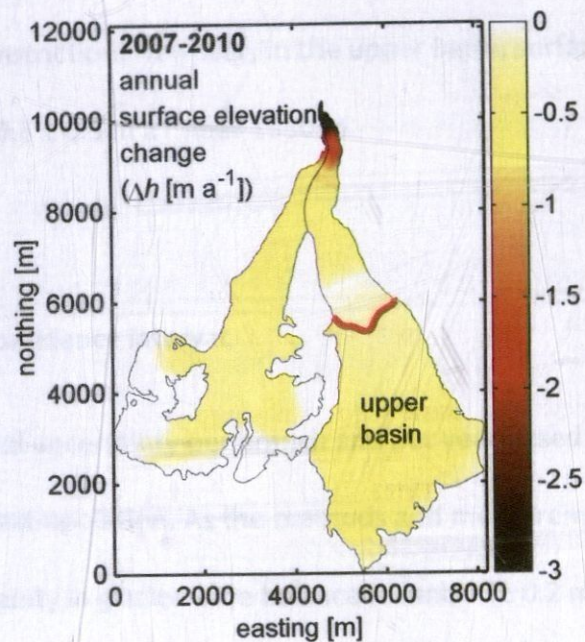


Figure 1.9. Thinning for 2007–2010 normalized per year. 1360 m contour (2010) in the main branch shown in red. The upper basin of the main branch (>1360 m) shows more thinning than the area just below 1360 m. This is similar to the 1957–2010 pattern in figure 6.

to 16 September, 2010. Adjusted volume change over the same interval is estimated by summing surface elevation change over the surface of the glacier then normalizing by the average glacier area.

The total volume change on Eklutna Glacier from 2007–2010 was $-3.8 \pm 1.4 \times 10^7 \text{ m}^3$. Normalization by the average glacier area yielded an average elevation change of $-1.3 \pm 0.5 \text{ m}$, and a mean annual thickness change of $-0.4 \pm 0.2 \text{ m a}^{-1}$ (Figure 1.9). The maximum surface elevation change was $-9.8 \pm 1.6 \text{ m a}^{-1}$ at the 2010 terminus. Below the upper basin surface elevation changes decreased with elevation to the minimum change of $-0.0 \pm 0.3 \text{ m a}^{-1}$ at 1300 m in the constriction. However, in the upper basin, surface elevation change increased again to $-0.8 \pm 0.5 \text{ m a}^{-1}$ near 1530 m.

1.4. Uncertainties

We report uncertainties at the 95% confidence interval.

Mass Balance – We calculate individual uncertainty per branch and per year based on both measurement error and spatial extrapolation. As the methods and measurements are similar each year the total uncertainty in glacier wide balance is similar ($\pm 0.2 \text{ m a}^{-1}$) each year. The smooth surface characterizing Eklutna Glacier allows repeatable stake height measurements to $\pm 0.02 \text{ m}$ and density measurements accurate to $\pm 5\%$.

Uncertainties due to spatial extrapolation are harder to quantify. We estimated that measurements are representative of the elevational mean to within $\pm 0.1 \text{ m}$ in the relatively smooth and homogeneous accumulation zone and $\pm 0.2 \text{ m}$ in the rougher and

more heterogeneous ablation zone. Mass balance measurements at secondary sites are consistent with those estimates. For areas above and below the range of sites we also account for the uncertainty in the slope of the balance gradient by including a factor equal to the difference in mass balance from the slope calculated in 2008 and 2010 (again disregarding 2009 because of the tephra). Our uncertainty in the ELA position arises from both the variance in the ELA elevation due to topography and the uncertainty in precisely locating the ELA on the DEM. Final uncertainties were calculated using standard propagation of error methods (Bevington and Robinson, 2003).

Glacier Surface Elevation Change – For the comparison of 1957 to 2010 we used the stated uncertainties in each DEM and we assume the s.e. of the residuals in off glacier areas approximate the uncertainty in the vertical transform. The glacier-wide uncertainty (± 33 m) is largely driven by the uncertainties in the 1957 maps (section 2.2.). The uncertainty in the 2007–2010 thickness change is significantly more complicated because of the spatial nature and the adjustments for ablation and emergence over summer 2007. We estimate total glacier-wide uncertainty of ± 0.5 m. We account for all of the uncertainty components individually and weight them by the relative contribution to the final product using standard error propagation methods (Appendix 3; Bevington and Robinson, 2003). We use the standard deviation (σ) of the residuals in off glacier areas to estimate the uncertainty of the within bin comparisons (i.e. the potential for a local skew to the data), we use the standard methods to quantify the uncertainty in the predicted ablation for 2007 based on the regression variances

(Bevington and Robinson, 2003), the previously calculated uncertainty in mass balance, and finally we estimate the uncertainty in the spatial variance within a given bin with the variance within that bin.

Finally we note that the uncertainty calculations for the 2007–2010 surface elevation change in the west branch are based on a single profile and likely underestimate the within-bin variability.

1.5. Comparison of methods

Albeit with large uncertainty, we made a comparison of direct mass balance measurements with surface elevation change data over the 2007–10 interval, under the assumptions that internal and basal mass balance terms are minor (Trabant and Mayo, 1985; Cuffey and Patterson 2010), and that surface elevation changes represent a gain or loss of ice (e.g., Sorge's Law; Bader, 1954). We imposed the constraint that glacier-wide emergence sums to zero (Cox and March, 2003; Holmlund, 1988; step 5, above).

Table 1.2. September 2007 to September 2010 mean ice thickness change based on change in surface elevation (Δh), and mass balance (B).

	entire glacier	main branch	west branch
mean Δh , [m]	-1.3 ± 0.5	-1.6 ± 0.4	-0.9 ± 0.5
B [m ice]	-1.3 ± 0.3	-1.6 ± 0.2	-0.9 ± 0.4

We found that the methods agreed and yield a three-year volume change of $-3.8 \times 10^7 \text{ m}^3$ (Table 1.2). The agreement between these mostly independent methods suggests that volume changes are well resolved.

1.6. DISCUSSION

The total magnitude of surface elevation change in and near the accumulation zone of the main branch is -1.4 ± 0.9 and $-0.8 \pm 0.5 \text{ m a}^{-1}$ for the periods 1957–2010 and 2007–2010, respectively. Some amount of accumulation zone thinning could occur on any glacier as part of a typical stable response to a perturbation in climate, but we will show that Eklutna Glacier is responding to climatic changes in an unstable way that has important implications for its future mass balance. To accomplish this we will look at the 2010 AAD and the change in AAD 2008–10. Then we will put the 2008–10 mass balance into temporal context by comparing it to the 46 year mass balance record from nearby Wolverine Glacier. Finally we will use mass continuity to compare the balance flux to the thinning flux, and examine the magnitude of the imbalance between the mass inputs and the present glacier geometry. We will discuss the stability of the 2010 geometry in the 2008–10 climate and the implications for the glacier's future contributions to water resources.

1.6.1. Area Altitude Distribution Change

In the main branch the observed thinning 2008–10 is acting to convert regions of the accumulation area to ablation zone (Figure 1.10a). This effect is exacerbated by several

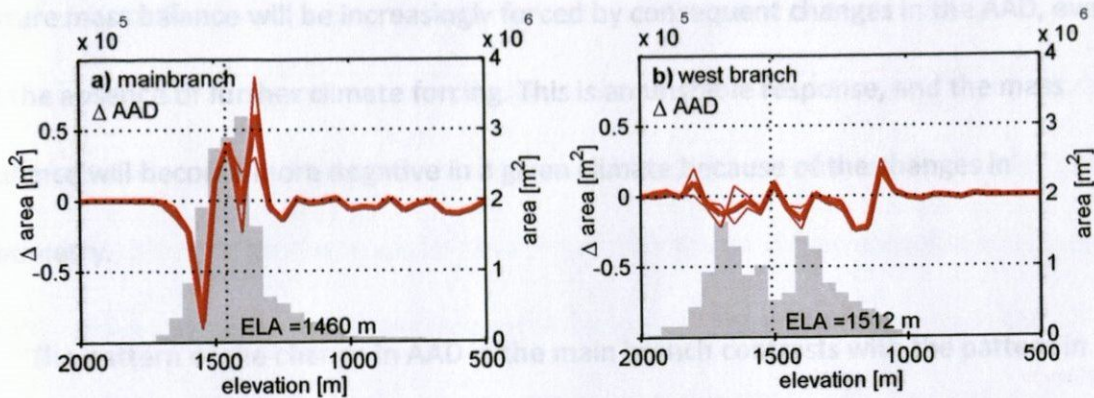


Figure 1.10. The change in area altitude distribution (AAD) (red, left axes) and the AAD (grey, right axes) for September 2007 to September 2010 in the main branch (a) and the west branch (b). Note the different scale. Surface elevation change in the main branch is reducing the area above the 2008–10 ELA (1460 m) and increasing the area below the ELA. In the west branch the changes in the AAD are less significant, especially above the 2008–10 ELA of 1490 m.

factors. The bulk of the AAD in the main branch is concentrated between 1350 and 1550 m, the area we have already labeled as the upper basin. The upper basin is very flat with an average slope of $\sim 2^\circ$ (rise/run ~ 0.035), so small shifts in the surface elevation result in large horizontal shifts in surface contour location. The 2008–10 cumulative ELA was located at 1460 m, coincident with the peak in the AAD at 1450–1500 m. The combination of these two factors results in small amounts of thinning in the upper basin changing the accumulation rate. As an example, if we apply the 2010 balance profile to the 2007 geometry, the resulting accumulation area is 2% larger than the 2010 accumulation area, and the resulting total accumulation is 3% greater than the 2010 accumulation. So the geometric changes 2008–10 resulted in a glacier with less accumulation for a given climatic forcing. If the 2008–10 pattern of thinning continues,

future mass balance will be increasingly forced by consequent changes in the AAD, even in the absence of further climate forcing. This is an unstable response, and the mass balance will become more negative in a given climate because of the changes in geometry.

The pattern of the change in AAD in the main branch contrasts with the pattern in the west branch (Figure 1.10). The area in the west branch is distributed over a larger elevation range with a bimodal distribution. The 2008–10 cumulative ELA is in between the peaks in the AAD, and the steeper surface slopes result in smaller horizontal displacements for a given quantity of thinning. Finally, the thinning is less at higher elevations. These factors combine so that the effects of thinning on the AAD do not result in a reduced accumulation area for a given climatic forcing.

Rather than a stable response where the accumulation area ratio (AAR) is returned to stable condition through terminus retreat (Nye, 1960; Jóhannesson and others, 1989; Harrison and others, 2001), continued accumulation zone thinning will promote a feedback that forces the glacier further from equilibrium. As thinning converts progressively more of the accumulation area into the ablation zone, the reduction in mass balance inputs eventually result in flow stagnation. Böðvarsson (1955) pointed out that this instability is inherent on glaciers with a sufficiently flat bed. The decrease in ice thickness results in a decrease in ice flux due to the elevation-dependent surface balance rate. This perpetuates a positive feedback between decreasing ice flux and

decreasing ice thickness, which, in turn results in continued decreases in glacier volume and length. If the feedback continues it ultimately results in flow stagnation and surface wastage. While the main branch of Eklutna does have a steep terminus, the thinning in the upper basin is reminiscent of the Böðvarsson instability. The present terminus is at 530 m where the surface mass balance rates are -10 to -12 m a^{-1} , so changes in the terminus geometry should, in theory, be able to bring the present glacier back into equilibrium. However, the narrowness of the lower reaches of the glacier limits the potential stabilizing effect of changes in terminus position as we will address further in 4.3.

1.6.2. Long-Term Trends in Mass Balance

The 43-year mass balance record assembled at Wolverine Glacier, located 80 km to the south in a similar climate (van Beusekom and others, 2010), provides context for our short-term record (Figure 1.11). Interannual variability is large; all three years are characterized by above-average snowfall, but summers ranged from wet with below-average temperatures to above-average temperatures (<http://www.ncdc.noaa.gov/>) and compounded by widespread tephra deposition in 2009 (Schaefer, 2011). Through this short period, we found that the balance series collected at both glaciers are similar in both relative amplitude and timing (Figure 1.11a). This suggests that the longer duration time series from Wolverine Glacier forms a reasonable first-order proxy for the balance history at Eklutna Glacier (Figure 1.11b). Mean mass balance at Wolverine

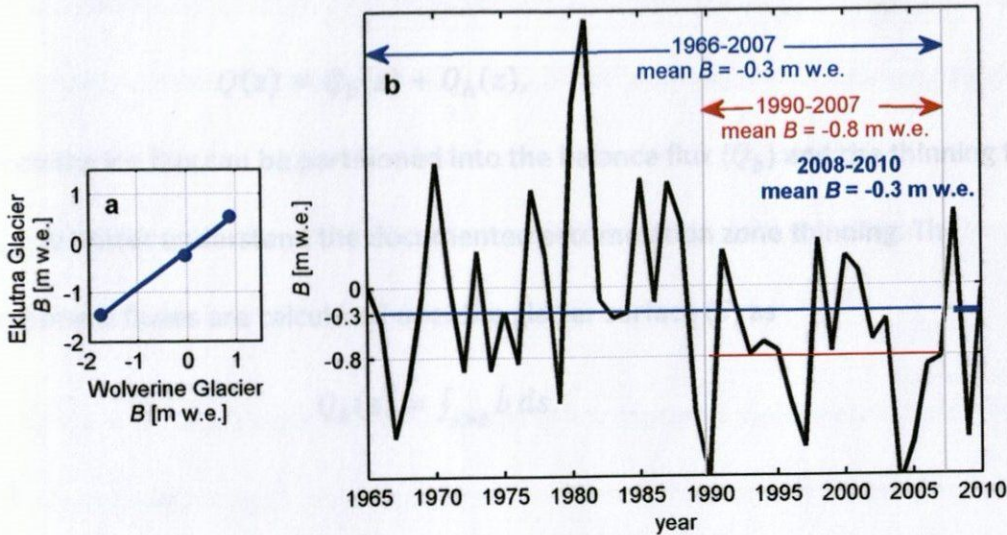


Figure 1.11. a) The mass balances on Eklutna Glacier has a consistent relationship (although slightly less variability) to Wolverine Glacier in 2008–10. b) The black line shows the 44 years of mass balance record on Wolverine glacier. The mean mass balance 1966–2007 is -0.3 m a^{-1} . However, for the 20 years 1988–2007 the mean value is -0.8 m a^{-1} . 2008–10 mean value is -0.3 m a^{-1} , suggesting that the mass balance 2008–10 is similarly negative to the long term record and a positive anomaly over the immediate preceding years.

Glacier 2008–10 is -0.3 m a^{-1} , nearly exactly the same as the mean for the entire 43 years of -0.3 m a^{-1} , and a significant positive anomaly compared to the mean mass balance value of -0.8 m a^{-1} from 1990 to 2007. Likelihood is high that both glaciers experienced a more positive mass balance interval during this study than during the previous 20-years. We consider this as we continue to analyze the long-term and short-term records of accumulation zone thinning at Eklutna Glacier using mass continuity.

1.6.3. Continuity and Ice Flux

Following Brown and others (1982), we evaluate the mass continuity equation for ice flux (Q) passing under a given surface elevation (z) as

$$Q(z) = Q_b(z) + Q_h(z), \quad (4)$$

where the ice flux can be partitioned into the balance flux (Q_b) and the thinning flux (Q_h) to better understand the documented accumulation zone thinning. The component fluxes are calculated over the glacier surface (S) as

$$Q_b(z) = \int_{s>z} \dot{b} ds, \quad (5)$$

and

$$Q_h(z) = - \int_{s>z} \dot{h} ds \quad (6)$$

(Rasmussen and Meier, 1982).

In steady state, $\dot{h} = 0$, and ice flux is equal to the balance flux ($Q = Q_b$). Our previous definition of stability as a geometric change that returns the mass balance toward equilibrium has implications for ice flux. In a stable response to a perturbation in climate, ice-flux will either increase or decrease to achieve a new equilibrium with the balance flux; consequently the ice-flux at any given time should be at some intermediate value between some prior balance flux (that the present geometry is at least partially a product of) and the present balance flux. Eventually the decrease (or increase) in flux causes retreat (or advance) at the terminus which has a stabilizing effect as it brings the glacier back toward steady state. Both tidewater (Meier and Post, 1987) and surging glaciers (Kamb and others, 1985; Murray and others, 2000) are known to enter periods of instability forced by ice dynamics, where the changes in ice-flux

result in geometric changes that alter surface mass balance to a much greater degree than changes in climate. However, the mass balance of terrestrial, non-surging glaciers is considered to be a function of climate with some lag or response time (Nye, 1960; Jóhannesson and others, 1989; Harrison and others, 2001; Luthi, 2009), and dynamics are generally ignored.

We plot the flux terms for each branch as a function of surface elevation in Figure 1.12. In the main branch, accumulation zone thinning is presently supporting half of the calculated ice flux at the ELA, and all of the ice flux out of the upper basin. Such a pattern is absent in the west branch, where the balance flux supports the majority of flow out of the accumulation zone, and thinning only contributes noticeably to the total

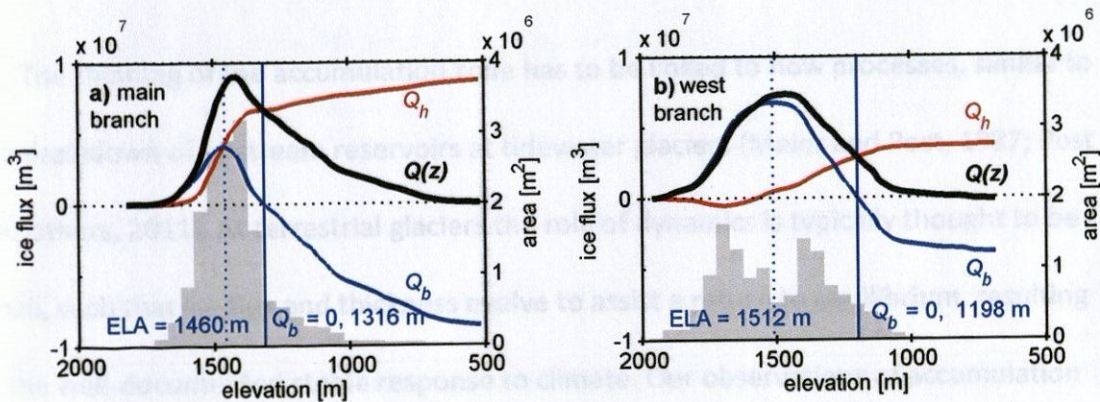


Figure 1.12. 2008–10 ice flux ($Q(z)$) calculated from the thinning flux (Q_h) and the balance flux (Q_b) are plotted on the left axes, and AADs plotted on the right axis. In the main branch (a) the total flux exceeds the balance flux even in the accumulation zone. The balance flux drops to 0 at 1300 m, so a glacier in equilibrium with 2008–10 climate would terminate >1300 m. In the west branch (b) the total ice flux is less than the balance flux in most of the accumulation zone, and the thinning flux only significantly contributes to the total flux at lower elevations. The balance flux drops to 0 at 1200 m, so the 2008–10 climate would support a relatively larger glacier in the west-branch with a terminus >1200 m.

flux on the lower glacier (Figure 1.12b). Presently the balance flux in the main branch equals zero > 1300 m, indicating that an equilibrium glacier in the present climate would have a terminus within the confines of the upper basin. This represents a terminus retreat of > 5 km, more than half the length of the present glacier.

In the context of the Wolverine Glacier mass balance record the results in the main branch are particularly striking. It seems unusual that a glacier of this size would be this far from equilibrium if 2008–10 is actually less negative than the previous 20 years of mass balance. This suggests that ice flux to the lower glacier has largely been supported by thinning in the upper basin for at least the previous 20 years and possibly longer.

The thinning of the accumulation zone has to be linked to flow processes, similar to the drawdown of upstream reservoirs at tidewater glaciers (Meier and Post, 1987; Post and others, 2011). At terrestrial glaciers the role of dynamics is typically thought to be small, such that ice flux and thickness evolve to assist a return to equilibrium, resulting in the well-documented stable response to climate. Our observations of accumulation zone thinning suggest that future reductions in ice flux are inevitable, and that a period of rapid and dramatic retreat will ensue. A full assessment of the three dimensional geometry and flow-field is presently underway to understand the conditions that are presently enabling accumulation zone thinning and constrain the future behavior of the system.

1.6.4. Broader implications

We need to understand the forcing mechanism on the main branch of Eklutna Glacier in order to postulate how common this type of instability is. If it is common it has significant ramifications for predictions based on linearized relationships. Linearized response time theories (e.g. Johannesson and others, 1989; Harrison and others, 2001) are widely used to describe the macro-response of non-calving mountain glacier geometries to changes in climate. The use of volume-area scaling (Chen and Ohmura, 1990; Bahr and others, 1997) to predict future geometry of a given glacier (e.g., Möller and Schneider, 2010) is clearly problematic, but if this kind of instability is common it also has ramifications for the broader use of scaling to predict phenomenon like global sea level rise (e.g., Van de Wal and Wild, 2001; Radic and Hock, 2010).

1.7. SUMMARY

The glacier-wide surface mass balance for 2008–10 was -1.3 ± 0.3 m of ice. This corresponds well to the direct measurement of mean surface elevation change of -1.3 ± 0.5 m. Over 60% of the 2008–10 volume change is generated by thinning in and near the accumulation zone. The change in the AAD shows that the thinning in the upper basin is converting areas that were previously in the accumulation area to the ablation zone. The decrease in surface mass balance around the ELA decreases the probability of positive mass balance years in the future.

Comparison to the 46 year mass balance record at Wolverine Glacier suggests that 2008–10 likely had less negative mass balance than the preceding 20 years. The 2008–10 balance flux shows that the lower 5 km of this 10 km long glacier is presently supported by accumulation zone thinning.

In aggregate these results suggest that the modest changes in surface elevation within the upper basin of $-0.8 \pm 0.5 \text{ m a}^{-1}$ will force future mass balance to be more negative in a given climate and are the product of a flow regime that is at least unusually insensitive to surface mass balance inputs. Despite the fact that the effects are not as impressive as a typical surge or tidewater glacier retreat, this relationship between climate and geometry defines instability in the mathematical sense. Resolving the apparent insensitivity of ice flow processes to the mass balance inputs requires a detailed investigation of the glacier geometry and the resistive stresses governing ice flow out of the upper basin. Only then can we evaluate if a return to a stable geometry is likely.

Acknowledgements

Thanks to Jason Geck for reviewing the manuscript. Special thanks to John Sykes, all the students of Alaska Pacific University's annual Glaciology and Glacier Travel field courses, and to everyone else who helped with fieldwork. Thanks to NASA for an Earth and Space Science Fellowship, Anchorage Municipal Light and Power and James Posey for funding most of the fieldwork, the NIWR for funding many of my field assistants, and Anchorage

Water and Wastewater Utility for logistical assistance. Thanks to SPIRIT (Spot 5 stereoscopic survey of Polar Ice: Reference Images and Topographies; Korona and others, 2009) for use of the SPOT image, and to the Mat-Su Salmon Partnership for the 2010 LiDAR. Also thanks to Janet Curran at the USGS for convincing the Mat-Su Salmon Partnership that Eklutna Glacier LiDAR was a useful addition to their larger LiDAR project. Thanks to Martin Truffer for helpful discussion on emergence.

References

- Aðalgeirsdóttir, G., K.A. Echelmeyer, and W.D. Harrison. 1998. Elevation and volume changes on the Harding Icefield, Alaska. *J. Glaciol.*, **44**(148), 570-582.
- Arendt, A.A., K.A. Echelmeyer, W.D. Harrison, C.S. Lingle, and V.B. Valentine. 2002. Rapid wastage of Alaska glaciers and their contribution to rising sea level. *Science*, **297**(382), 382 – 386.
- Bader, H. 1954. Sorge's law of densification of snow on high polar glaciers. *J. Glaciol.*, **8**(52), 3-7.
- Bethier, E., E. Schiefer, G.K.C. Clarke, B. Menounos, and F. Rémy. 2010. Contributions of Alaska glaciers to sea-level rise derived from satellite imagery. *Nature Geoscience*, **3**, 92-95.
- Bevington, P.R., and D.K. Robinson. 2003. *Data reduction and error analysis for the physical sciences*. New York, N.Y., McGraw-Hill.
- Böðvarsson, G. 1955. On the flow of ice-sheets and glaciers. *Jökull.*, **5**, 1-8.
- Brown, C.S., M.F. Meier, and A. Post. 1982. Calving speed of Alaska tidewater glaciers, with application to Columbia Glacier. *USGS Prof. Paper*, 1258-C.
- Cogley, J.G. and 10 others. 2011. *Glossary of glacier mass balance and related terms*. IHP-VII Technical Documents in Hydrology 86. IACS 2. UNESCO-IHP, Paris.
- Cox, L.H., and R.S. March. 2004. Comparison of geodetic and glaciological mass-balance techniques, Gulkana Glacier, Alaska, U.S.A. *J. Glaciol.*, **50**(170), 363-370.

- Cuffey, K.M., and W.S.B. Patterson. 2010. *The physics of glaciers*, 4th ed. Oxford, etc. Elsevier.
- Echelmeyer, K.A., and 8 others. 1996. Airborne surface profiling of glaciers: a case-study in Alaska. *J. Glaciol.*, **42**(142), 538-547.
- Gesch, D., M. Oimoen, S. Greenlee, C. Nelson, M. Steuck, and D. Tyler. 2002. The National Elevation Dataset. *Photogrammetric Engineering and Remote Sensing*, **68**, 5-11.
- Glen, J.W. 1952. Experiments on the deformation of ice. *J. Glaciol.*, **2**(12), 111-114.
- Harrison, W.D., D.H. Elsberg, K.A. Echelmeyer, and R.M. Krimmel. 2001. On the characterization of glacier response by a single time-scale. *J. Glaciol.*, **47**(159), 659-664.
- Holmlund, P. 1988. Is the longitudinal profile of Storglaciären, northern Sweden, in balance with the present climate? *J. Glaciol.*, **34**(118), 269-273.
- Hubbard, B., and N. Glasser. 2005. *Field techniques in glaciology and glacial geomorphology*. West Sussex, England, John Wiley & Sons.
- Hutter, K. 1981. The effect of longitudinal strain on the shear stress of an ice sheet: in defence of using stretched coordinates. *J. Glaciol.*, **27**(95), 39-56.
- Johannesson, T., C. Raymond, and E. Waddington. 1989. Time-scale for adjustment of glaciers to changes in mass balance. *J. Glaciol.*, **35**(121), 355-369.
- Kamb, B., and 7 others. 1985. Glacier surge mechanism: 1982-1983 surge of Variegated Glacier, Alaska. *Science*, **227**(4686), 469-479.
- Korona, J., E. Berthier, M. Bernard, F. Rémy, E. Thouvenot. 2009. SPIRIT. SPOT 5 stereoscopic survey of Polar Ice: Reference Images and Topographies during the fourth International Polar Year (2007-2009). *ISPRS J. of Photogrammetry and Remote Sensing*, **64**, 204-212.
- Larquier, A.M. 2011. Differing contributions of heavily and moderately glaciated basins to water resources of the Eklutna Basin, Alaska. (M.S. thesis. Alaska Pacific University).

- Luthi, M.P. 2009. Transient response of idealized glaciers to climate variations. *J. Glaciol.*, **55**(193), 918-930.
- Meier, M.F., M.B. Dyurgerov, and G.C. McCabe. 2003. The health of glaciers: recent changes in glacier climate.
- Meier, M.F., and A. Post. 1987. Fast Tidewater Glaciers. *J. of Geophysical Research*. **92**(B9) 9051-9058.
- Moran, E.H., D.L. Galloway. 2006. Ground-water in the Anchorage Area, Alaska – Meeting the challenges of ground-water sustainability. *USGS Fact Sheet*, 2006-3148.
- Murray, T., G.W. Stuart, P.J. Miller, J. Woodward, A.M. Smith, P.R. Porter, and H Jiskoot. 2000. Glacier surge propagation by thermal evolution at the bed. *J. of Geophysical Research*, **105**(B6), 13,496-13,507.
- Neal, C. A., McGimsey, R. G., Gardner, C. A., Harbin, M. L., and Nye, C. J. 1995. Tephra-fall deposits from the 1992 eruptions of Crater Peak, Mount Spurr volcano, Alaska: a preliminary report on distribution, stratigraphy, and composition. In Keith, T. E. C. (ed.). *The 1992 eruptions of Crater Peak Vent, Mount Spurr volcano, Alaska, U.S. Geological Survey Bulletin B 2139*, p. 65-79.
- Nye, J.F. 1952. The mechanics of glacier flow. *J. Glaciol.*, **2**(12), 82-93.
- Nye, J.F. 1960. The response of glaciers and ice-sheets to seasonal and climatic changes. *Proceedings of the Royal Society of London*, **256**(1287), 559-584.
- Post, A., S. O'Neel, R.J. Motyka, and G. Streveler. 2011. A complex relationship between calving glaciers and climate. *EOS, Transactions of the American Geophysical Union.*, **92**(37), 305-312.
- Rasmussen, L.A., and M.F. Meier. 1982. Continuity Equation Model of the Predicted Drastic Retreat of Columbia Glacier, Alaska. *USGS Prof. Paper*, 1258-A.
- Roman, D.R., Y.M. Wang, J. Saleh, X. Li. 2009. Final national models for the United States: Development of GEOID09. *NGS Prof. Paper*.
- Schaefer, J.R.G., ed. 2011. The 2009 Eruption of Redoubt Volcano, Alaska. *Alaska Division of Geological & Geophysical Surveys Report of Investigations*. 2011-5, __ p., in press.
- Schwitzer, M.P., and C.F. Raymond. 1993. Changes in the longitudinal profiles of glaciers during advance and retreat. *J. Glaciol.*, **39**(133), 582-590.

Trabant, D.C. and L.R. Mayo. 1985. Estimation and effects of internal accumulation on five glaciers in Alaska. *Ann. Glaciol.*, **6**, 113-117.

Van Beusekom, A.E., S. O'Neel, R.S. March, L.C. Sass, and L.H. Cox. 2010. Re-analysis of the Alaskan benchmark glacier mass balance data using the index method. *USGS Sci. Invest. Rep.*, 2010-5247.

Weertman, J. 1961. Stability of ice-age ice sheets. *J. Geophys. Res.*, **66**(11), 3783-3792.

Appendix 1.1. Mass balance measurements

Accumulation (c_{sfc}), ablation (a_{sfc}) and surface balance (b_{sfc}) measurements, 2008 – 2010.

Year	Elevation m	c_{sfc} m w.e.	Date spring trip	a_{sfc} m w.e.	Date fall trip	b_{sfc} m w.e.
2008	955.9	0.07	10 may	-4.57	20 Sept.	-4.50
	1215.1	1.41	13 May	-1.76	21 Sept.	-0.35
	1431.0	1.83	8 May	-1.11	27 Sept.	+0.72
2009	1130.4	0.60	9 May	-4.77	11 Sept.	-4.17
	1393.9	1.42	12 May	-3.64	12 Sept.	-2.22
	1530.8	1.64	8 May	-1.67	12 Sept.	-0.03
2010	1130.6	0.96	24 May	-3.94	21 Sept.	-2.98
	1394.7	2.05	21 May	-2.07	21 Sept	-0.02
	1530.6	2.47	26 May	-1.81	22 Sept	+0.66

Appendix 2. Datum adjustment

The datum adjustment is based on comparison of low-angle low-topography minimally-vegetated off-glacier terrain in two separate areas that bracket the glacier. We compare laser altimetry points to the 2.5 m LiDAR DEM using a bilinear interpolation. Down valley of Eklutna Glacier 2454 points have a mean offset of -0.494 m (s.e. 0.009 m), and down valley from Eagle Glacier (an area ~3.5 km south of the accumulation zone of Eklutna) 2171 points have a mean offset of -0.504 m (s.e. 0.013 m). Because the values are very similar we assume a constant z transform for the mean offset for both areas at -0.499 (s.e. 0.008 m). The variance in this comparison gives us an estimate of the potential systematic errors in on glacier areas.

Appendix 3. Propagation of errors

When final values are based on a function of component variables (e.g. section 3.2) the uncertainties combine as follows

$$X = f(x_1, x_2, \dots, x_n), \quad (\text{A1})$$

Where the variance (σ^2) in X is related to the variance in the various component variables x_1, x_2, \dots, x_n weighted by the functional dependence of X on each component variable

$$\sigma_X^2 = \sum_{i=1}^n \sigma_i^2 \left(\frac{\partial f}{\partial x_i} \right)^2 \quad (\text{A2})$$

(Bevington and Robinson, 2003).

Mark A. Cook,¹ Max Ormel,² Joseph A. MacGregor,³ Michael G. Leno,⁴

Stephen F. Price⁴

¹Alaska State University, 4200 University Dr. Anchorage, AK, 99508, USA

²Department of Earth and Planetary Science Center, 4210 University Dr, Anchorage, AK, 99508, USA

³Department of Geology, The University of Texas at Austin, Austin, TX, 78712, USA

⁴Los Alamos National Laboratory, Los Alamos, NM, 87545, USA

ABSTRACT. Eklutna Glacier is a small mountain glacier in southcentral Alaska with a complex spatial distribution of volume change. 65% occurs in and near the supraglacial zone. Surface elevation change high on the glacier exceeds that measured in the middle of the glacier. We characterize the flow field and basal geometry associated with this enhanced thinning to understand ongoing retreat. The medial upper basin is over-deepened up to 100 m and is separated from the lower glacier by a prominent regel. Compounded by lateral incision, the cross-sectional area is reduced by 65% over a horizontal distance of 1.5 km above the regel. Velocities increase from $\sim 20 \text{ m a}^{-1}$ near the margin to $\sim 60 \text{ m a}^{-1}$ above the regel. We use a top-down force balance approach to infer the stresses from velocity measurements. In the upper

Chapter 2: Ice geometry and motion associated with enhanced thinning in the accumulation-zone of Eklutna Glacier, Alaska

Louis C. Sass,^{1,2} Shad O'Neel,² Joseph A. MacGregor,³ Michael G. Loso,¹

Stephen F. Price⁴

¹*Alaska Pacific University, 4200 University Dr, Anchorage, AK, 99508, USA*

²*United States Geological Survey Alaska Science Center, 4230 University Dr, Anchorage, AK, 99508, USA*

³*Institute for Geophysics, The University of Texas at Austin, Austin, TX, 78758, USA*

⁴*Los Alamos National Laboratories, Los Alamos, NM, 87545, USA*

ABSTRACT. Eklutna Glacier is a small mountain glacier in southcentral Alaska with an anomalous spatial distribution of volume change; 65% occurs in and near the accumulation zone. Surface elevation change high on the glacier exceeds that measured in the middle of the glacier. We characterize the flow-field and basal geometry associated with this enhanced thinning to understand ongoing changes. The broad upper basin is overdeepened up to 100 m and is separated from the lower glacier by a prominent riegel. Compounded by lateral convergence the cross-sectional area is reduced by 65% over a horizontal distance of 1350 m above the riegel. Velocities increased from $\sim 20 \text{ m a}^{-1}$ near the present ELA to $> 60 \text{ m a}^{-1}$ above the riegel. We use a top-down force balance approach to partition the stresses from velocity measurements. In the upper

basin the driving stress is ~ 80 kPa, however basal drag is only ~ 40 kPa, so the stress-gradient terms are important in governing flow out of the upper basin. Longitudinal drag is in phase with the driving stress, showing that the changes in ice thickness and cross sectional area are more important in the pattern of flow than changes in driving stress. As a result of the strongly convergent valley geometry, dynamic processes contribute substantially to the glacier response to climate by maintaining an extended terminus, advecting ice to low elevations where ablation rates are high. Simultaneously the thinning in the upper basin shifts the AAD lower.

2.1. INTRODUCTION

Mountain glacier dynamics are often thought to play a minor role in glacier mass balance and response to climate. Changes in glaciers are often predicted using mass or energy balance in conjunction with area-volume scaling (e.g., Möller and Schneider, 2010). The non-linearity in the stress-strain relationship (Glen, 1952), dictate that large changes in ice-flux can be accommodated with minimal changes in ice thickness (Fowler and Larsen, 1978; Hutter, 1981). Consequently mountain glaciers adjust to new climate regimes with advance or retreat of the terminus, and at least for small changes in climate the relationship between terminus position and climate is close to linear (Johannesson and others, 1989; Harrison and others, 2001; Oerlemans and others, 2001; etc.). Instabilities in the glacier-geometry climate relationship can occur when

dynamic processes force changes in geometry. Examples include tidewater glacier retreat (Meier and Post, 1987), surges (Kamb and others, 1985), and the Böttvarsson (1955) type instability. In each of these cases the relative size of the accumulation zone and the ablation zone changes not due to a change in the vertical position of the balance profile (i.e. climate) but rather due to a change in the surface elevation of the glacier. In each of these cases the glacier thins to maintain a balance between the driving stress and the resistive stresses.

Eklutna Glacier is a small mountain glacier in southcentral Alaska (Figure 2.1) with a previously documented anomalous pattern of mass-loss with 65% of the 2008–10 mass coming from the upper basin of the main branch (Sass and others, 2012). Thinning rates in the upper basin are higher than those in the mid-section of the glacier. The area of enhanced thinning is critically coincident with both the present equilibrium line altitude (ELA) and a very broad, flat, basin; which results in the surface mass balance being highly sensitive to both changes in climate and to enhanced thinning in the upper basin. The forcing mechanism behind the thinning is not immediately obvious; it does not calve, it does not exhibit loop moraines or an advancing terminus indicative of a surge, and the 2010 terminus is >900 m below the 2008–10 equilibrium line altitude (ELA) so it cannot be undergoing the classic Böttvarsson (1955) type instability as it requires a flat bed.

Here we present datasets of ice thickness, and surface velocity with the intention of understanding the enhanced thinning in the upper basin of the main branch (Sass and others 2012). To this end we developed a spatially continuous three dimensional geometry, which we used to analyze the present stress field. We used mass continuity to estimate depth-averaged velocities from surface measurements. Derivatives of velocity yield strain rates and are related to the stress field by the constitutive relation. This top down method (van der Veen and Whillans, 1989) of stress partitioning reveals the importance of the geometric control provided by the bedrock geometry on ice flow. Our analysis suggests enhanced thinning is caused by the flow-contraction forced by the bedrock geometry.

2.1.1. Setting

Eklutna Glacier is 10.4 km long, 29.7 km² in area, and located in the western Chugach Mountains of Alaska (Figure 2.1; Sass and others, 2012). The main branch and a smaller west branch flow together to form a steep narrow trunk. Our work concentrates on the main branch as it flows through a broad, flat upper basin ($y = 2000\text{--}6300$), and then transitions to a steeper, narrower, trunk ($y = 6400$) before joining the west branch ($y = 7500$). The terminus is presently at 540 m elevation. The smaller west branch is steeper and flows from higher elevations.

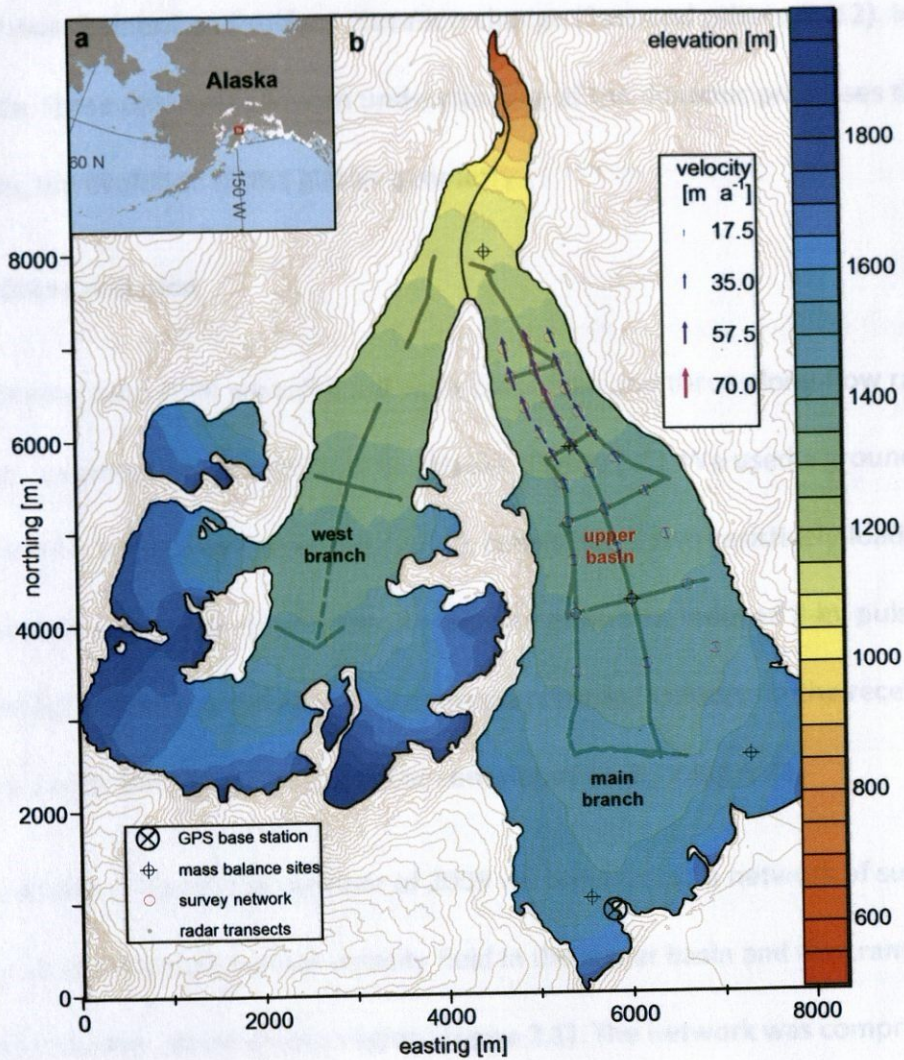


Figure 2.1. a) Location of Eklutna Glacier relative to Alaska. b) Map view of survey network, mass balance sites, and radar transects. The minimum easting and northing are subtracted from the Universal Transverse Mercator (UTM) coordinate system (zone 6N, WGS84) for simplification ($x = \text{UTM}_E - 388812$; $y = \text{UTM}_N - 6783612$). Topography is from 16 September, 2010 LiDAR. 50 m contour interval show the ice surface elevation. Velocity vectors are shown with arrows.

2.2. METHODS

New data presented in this study includes radar transects and repeat GPS surveys of a network of stakes (Figure 2.1). Fieldwork occurred in 2009, coincident with a three year

study of mass balance and surface elevation change (Sass and others, 2012). In aggregate, these data sets allow an understanding of the dynamic processes that are impacting the evolution of the glacier geometry.

2.2.1. Data Collection

Radar: During June 2009 we collected eight cross-flow and three along-flow radar transects covering both branches of the glacier (Figure 2.1). We used a ground-based system similar to Catania and others (2008), consisting of two resistively-loaded 5-MHz dipole antennas separated by ~50 m. An impulse generator induced 2-kV pulses into the transmitting antenna, and a digital oscilloscope recorded voltages in the receiving antenna. Single frequency GPS provided continuous positioning data.

Survey network: During the summer of 2009 we constructed a network of survey markers to characterize surface velocity field in the upper basin and the transition to the steeper, narrower, down-glacier region (Figure 2.1). The network was comprised of 3 x 10 markers in a quasi-regular grid. The center row of markers was aligned along the centerline of the glacier, and spaced to maintain at least one and not more than three anticipated ice thicknesses between nodes. We also installed a GPS monument and reference station on bedrock near the head of the glacier.

We used global positioning system (GPS) measurements to determine survey-marker positions (Figure 2.1) during three campaigns during summer of 2009 (June 6–7; June 29–30; July 31–August 1). A pair of dual-frequency receivers were used for post-

processed, static surveys (8–15 minutes) of each stake. We used precise-ephemeris the baseline processing against the local reference station and one or two continuously operating recording stations (CORS) located within 35 km of the glacier to generate closed loop solutions.

We also surveyed mass balance stakes two or more times per year from 2008–10 with single frequency GPS data post-processed against CORS stations. These poles were distributed along the centerline of the main branch, and two of them were co-located with 2009 survey network.

2.2.2. Analysis

Ice thickness: We calculated ice thickness from the radar returns. To improve the signal-to-noise ratio, we stacked sets of 512 radar traces together, which resulted in a typical horizontal posting of 2–4 m. The stacked traces were de-trended and then filtered using a 1–10 MHz band-pass filter. Two-way travel time was converted to depth using a constant wave speed of $167 \text{ m } \mu\text{s}^{-1}$.

Glacier Geometry: We utilized properties of ice deformation within a flow-following framework to construct a spatially continuous glacier geometry compatible with ice flow, a prerequisite to dynamical analyses (e.g., Seroussi and others, 2011). In the area between measured ice thickness transects the thickness model is well constrained and we used methods similar to Kavanaugh and others (2009) to interpolate ice thickness. Above the regions of radar measurements we utilized mass balance and surface

elevation change similar to Farinotti and others (2009) to extrapolate to the head of the glacier.

In between radar transects: Assuming simple shear, i.e the only nonzero deviatoric stress component is τ_{xz} , the flow relation can be integrated for ice flux (q) as

$$q = \langle u \rangle H = u_b H + \frac{2A}{n+2} \tau_b^n H^2, \quad (1)$$

where $\langle u \rangle$ is the depth-averaged velocity, H is the ice thickness, A is the rate factor, n is the exponent in the flow law, and τ_b is the basal drag (Cuffey and Patterson, 2010).

Consequently if $\tau_b \propto \tau_d$ then the flux depends on $H^5 \alpha^3$ (α is the surface slope, averaged over $\approx 1H$) if internal deformation (simple shear) is dominant, but simply on $u_b H$ if sliding dominates. Our analysis considered these two tractable end members and then used the observed thickness data to constrain our final estimate of H .

First we defined an approximately flow-following grid in order to facilitate interpolation. Then assuming linear variations in q along a given flow line we solved for H . In the cross-flow direction we compared the estimates of ice thickness generated by the two methods to the measured thickness on any along-flow profiles and calculated a factor φ that reproduced the measured H . We then applied φ (or the weighted average of φ between two along-flow transects) to that cross-flow row.

Downstream of the lowest cross-glacier transect we used the same method as outlined above by utilizing the zero-width zero-thickness cross-glacier profile at the

terminus. We assumed a constant value of φ on the lower glacier based on the lowest calculated values.

Above radar transects: ~30% of the area in the main branch and ~50% of the area in the west branch is located above the highest radar transects. Here, ice thickness estimates were made using methods similar to Farinotti and others (2009), by defining a series of one or more flow-lines from the head of each sub-basin down to a tie point at the highest cross-flow radar transect. The ice thickness is then solved as the solution to

$$H = \sqrt[n+2]{\frac{Q}{2A} \cdot \frac{n+2}{(C\rho g \sin\alpha)^n}} \quad (2)$$

Where Q is the "effective balance rate" (Farinotti and others, 2009) along each flow line equal to but with opposite sign the annual emergence rate (Sass and others, 2012). The empirically determined constant C , is derived for each flow-line at the tie point to the highest measured H .

All estimates of ice thicknesses were interpolated onto the same 10-m posts as the ice-surface DEM. We used a natural neighbor (Sibson, 1981) algorithm to preserve thickness around unevenly distributed data points and utilized the glacier margin (derived from the 2010 DEM; Sass and others 2012) as a zero-thickness boundary. The bed-elevation model is the ice-thickness model subtracted from the ice-surface DEM, after smoothing out pixel scale (10 m, primarily crevasses) features with a low-pass filter.

Flow Field: The stress-field can be resolved from measured stake displacements. Depth averaged velocity is essential and was accomplished using principles of mass continuity.

After calculating surface velocity from stake displacements we corrected these summer speeds to represent annual averages using the known scaling relation from annual surveys of mass balance sites. Next we constructed a series of flux gates along each cross-flow row in the survey network. Velocity profiles were extended across each gate to the no-flow margins using a cubic spline. Maximum ice-flux is bounded by the assumption that $\langle u \rangle = u_{sfc}$

$$Q_A = \sum u_{sfc} \cdot x_a, \quad (3)$$

where x_a is the cross-sectional area. Alternatively, we calculated ice-flux from continuity (Q_Ω) as

$$Q_\Omega = Q_b + Q_h, \quad (4)$$

Where Q_b is the cumulative contribution from surface mass balance and Q_h is the cumulative contribution from thinning over the total up glacier area (Brown and others, 1982; Sass and others, 2012). The ratio (ϕ) of the depth averaged velocity to the surface velocity can be estimated as

$$\phi = \frac{Q_\Omega}{Q_A}, \quad (5)$$

and is applied as a correction factor to the surface velocities

$$\langle u \rangle = \phi \cdot u_{sfc}. \quad (6)$$

After obtaining $\langle u \rangle$, we used an isoparametric finite element method (FEM; Cook and others, 2002) to calculate the horizontal strain rate tensor at the center of each nearly cubic element within the grid. This results in a new, inset, grid of 2×9 located at the original element centers.

Force Balance: The top down force balance (van der Veen and Whillans, 1989) assumes static equilibrium such that longitudinal drag (τ_L), side or wall drag (τ_W), and drag at the bed (τ_b), resist the driving stress (τ_d)

$$\tau_d = \tau_b + \tau_W + \tau_L \quad (7)$$

(Cuffey and Patterson, 2010). Using the resistive stresses (\bar{R}_{ij} ; van der Veen and Whillans, 1989) where x is along-flow, the stress gradient terms τ_L and τ_W are

$$\tau_L = -\frac{\partial}{\partial x} H \bar{R}_{xx}, \quad (8)$$

$$\tau_W = -\frac{\partial}{\partial y} H \bar{R}_{xy}. \quad (9)$$

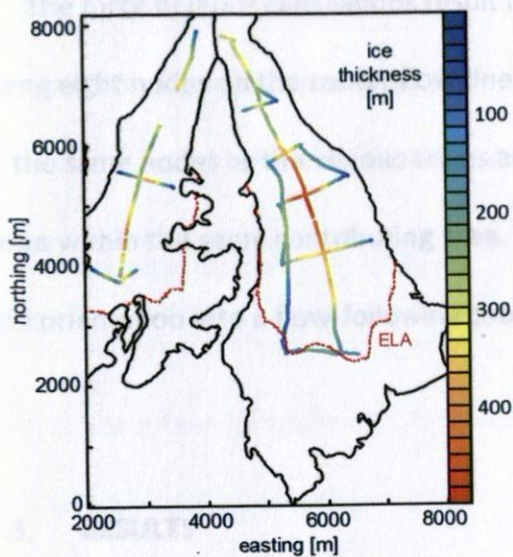


Figure 2.2. Map of measured ice thickness values obtained with 5 MHz radar. The approximate location of the mean ELA 2008–2010 is shown by the dashed line

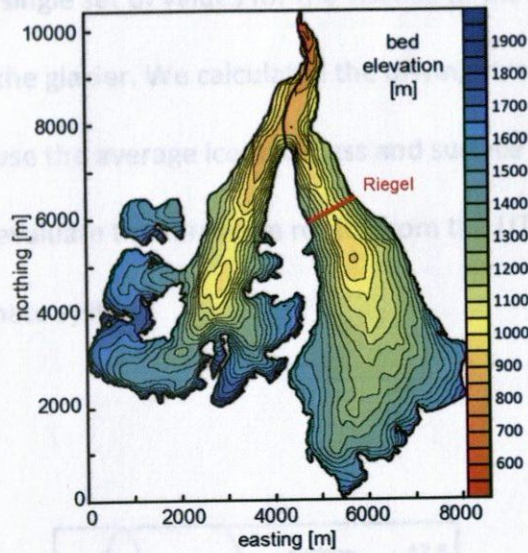


Figure 2.3. Bed elevation model derived from differencing a complete model of ice thickness from the surface DEM. 50 m contour interval. The upper basin in the main branch is separated from the lower glacier by a prominent bedrock riegel.

This ignores the \bar{R}_{zz} bridging term. The driving stress is calculated from ice thickness and surface slopes. Side wall-drag and longitudinal drag arise from the viscous properties of ice and can be calculated from a Glen type flow relation (Nye, 1957), and vertically integrated strain rates. These viscous terms dynamically link flow over distances of a few ice thicknesses (Kamb and Echelmeyer, 1986), and their effects are referred to as stress-gradient coupling (Cuffey and Patterson, 2010).

The force balance calculations result in a single set of values for the viscous terms along eight nodes on the center flow-line of the glacier. We calculated the driving stress at the same nodes as the viscous terms and use the average ice thickness and surface slope within the same contributing area. To evaluate the terms we rotate from the UTM grid orientation into a flow-following coordinate system.

2.3. RESULTS

Ice-thickness and Bed Geometry:

Maximum ice thickness (430 ± 15 m)

is located in the upper basin of the main branch (Figure 2.2). Down-glacier, the ice thickness rapidly

decreases to 260 ± 15 m. Bed

topography shows a riegel exists at

the constriction separating the upper

basin from lower glacier ($y = 6400$;

Figure 2.3). Above the riegel is a 2.1

km long section with up to 100 m of

over-deepening, coincident with the

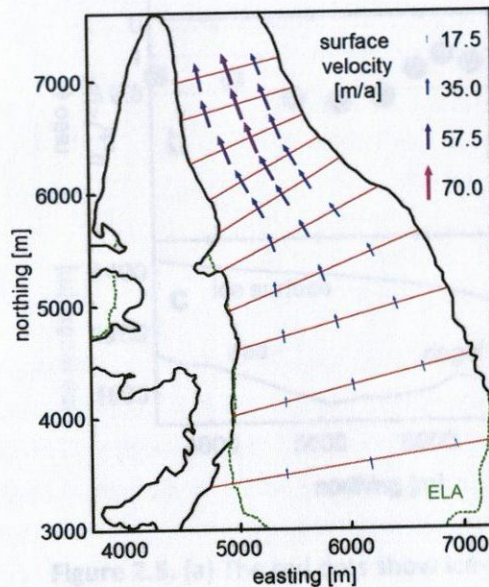


Figure 2.4. Eklutna Glacier surface velocities. Point velocities are determined from repeat GPS surveys. Within the survey network velocities represent the average velocity measured summer 2009. The approximate location of the mean ELA 2008–2010 is shown by the dashed line. The fine red lines show the gates used to calculate depth averaged velocities.

portion of the upper basin with the lowest surface slopes. In the 1350 m leading up to the riegel the cross-sectional area constricts from $4.4 \times 10^5 \text{ m}^2$ to $1.5 \times 10^5 \text{ m}^2$, a 65% reduction over < 4 centerline ice thicknesses. This defines a constricting reach of flow.

Ice Flow: Measured surface velocities generally increase down-glacier within the survey network (Figure 2.4). Motion is fastest along the centerline over the riegel ($y = 6400$; $66.1 \pm 0.2 \text{ m a}^{-1}$). In the upper portion of the network velocities are lower ($y = 3400$; $18.9 \pm 0.2 \text{ m a}^{-1}$).

Ice-flux calculations based on the assumption $\langle u \rangle = u_{sfc} (Q_A)$, are shown in Figure 2.5a. The maximum Q_A is coincident with the maximum overdeepening. The ice-flux calculated from continuity (Q_Ω ; Sass and others, 2012) peaks further up glacier. The ratio ϕ of $\langle u \rangle / u_{sfc}$ ranges from 0.74 to 1.02 (Figure 2.5b), with the lowest values occurring in the over-deepening and the

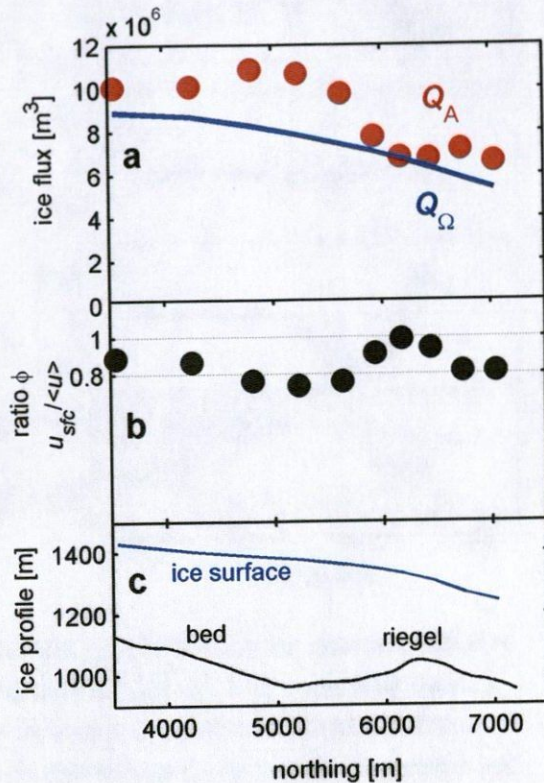


Figure 2.5. (a) The red dots show ice-flux from surface velocities (Q_A) at the flux gates in Figure 2.4 compared to the blue continuity based estimate of ice-flux (Q_Ω ; Sass and others, 2012). The ratio ϕ of the surface velocity to the depth averaged velocity is shown in (b). The dashed line at 0.8 is representative of a typical no-slip assumption, while the dashed line at 1 represents $\langle u \rangle = u_{sfc}$. (c) shows the centerline profile of glacier geometry.

highest values occurring at the
bedrock riegel.

The along-flow normal strain rate (based on the depth averaged velocities) in the upper part of the survey network is slightly negative (Figure 2.6b; $-9.0 \times 10^{-4} \text{ a}^{-1}$) indicating a small amount of compression. The strain rate steadily increases down glacier to a maximum of $3.8 \times 10^{-2} \text{ a}^{-1}$ at $y = 6000$, and then decreases again to a negative value of $-2.9 \times 10^{-3} \text{ a}^{-1}$ at $y = 6600$. The cross-flow normal strain-rates are consistently negative indicating compression (Figure 2.6c). However, the minimum value is $-9 \times 10^{-3} \text{ a}^{-1}$, so the cross-flow compression is smaller. The vertical normal strain rates are calculated from incompressibility, so in this situation they are nearly the inverse of the along-flow normal strain rates (Figure 2.6d).

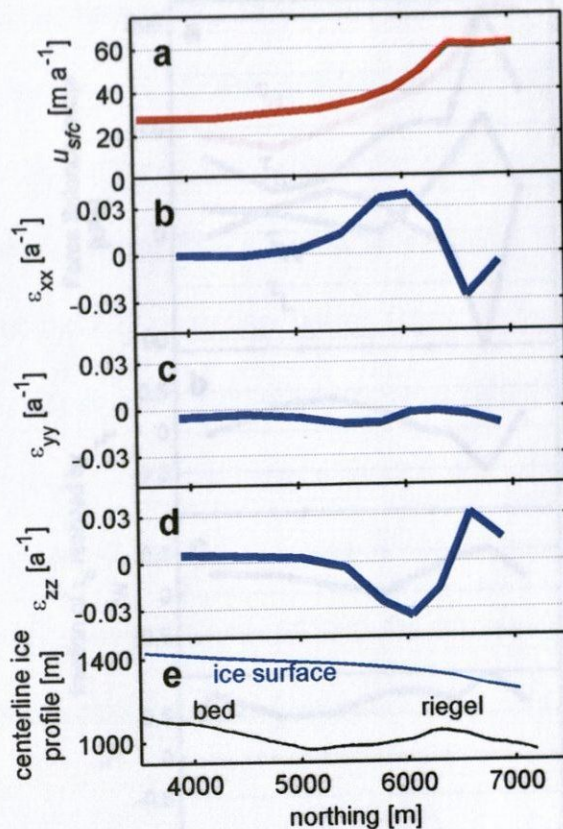


Figure 2.6. Centerline surface velocities (a, red) increase down glacier. The along-flow normal strain rate (b; averaged over the width of the grid) is extensional in the constricting reach and switches sign to compression downstream of the riegel. The cross-flow normal strain rates (c) consistently show compression, however, the values are smaller. Consequently the vertical normal strain rates (d) are nearly the inverse of the along flow rates. Panel (e) shows the centerline glacier geometry.

Force Balance: The values for each term in the force balance [equation (6)] are shown in Figure 2.7a. We follow the sign convention where the driving stress is positive, and positive values of the drag terms indicate resistance to flow. Negative values of the drag terms aid flow. Within the survey network area, the driving stress generally increases down-glacier, with the lowest values of +80 kPa just up-glacier of the thickest ice at $y = 4700$, and the highest values of +210 kPa above the riegel at $y = 6400$. Side drag shows a very minimal resistance to flow of 0 to 20 kPa in the upper basin increasing to a maximum resistance of 110 kPa as the ice passes across the riegel (Figure 2.7c). Resistance from longitudinal drag peaks near the thickest ice at 40 kPa,

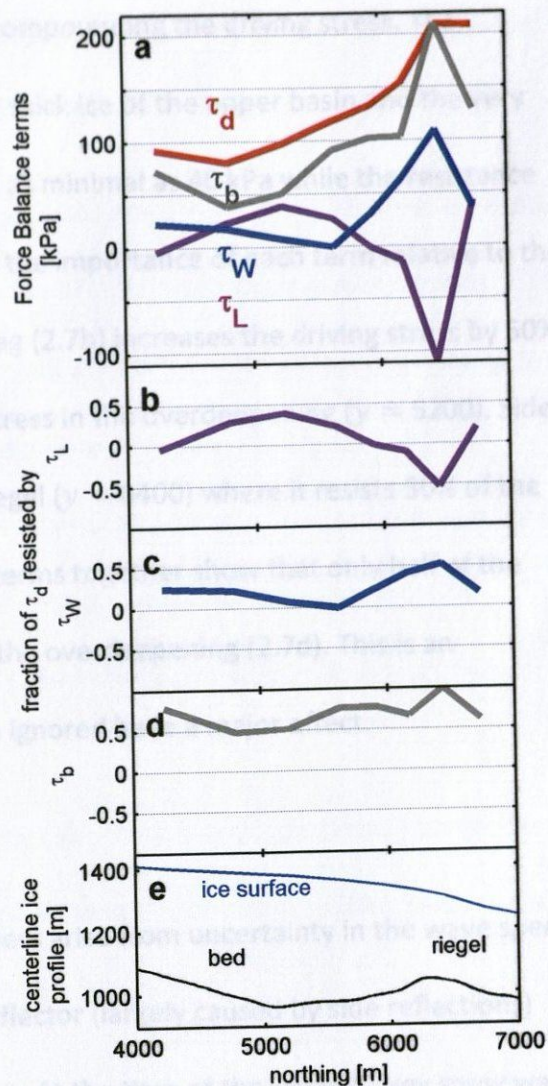


Figure 2.7. Force balance results along a central flow-line (a). The driving stress (τ_d , red) is balanced by side-wall drag (τ_W , blue), longitudinal drag (τ_L , fuschia), and basal drag (τ_b , grey). (b), (c), and (d) show the fraction of driving stress resisted by longitudinal drag, lateral drag, and basal drag. In the thick ice of the upper basin basal drag only supports 0.5 of the driving stress. Centerline ice profile along the same flow-line (e).

and then switches to -110 kPa at the riegel, compounding the driving stress. The residual term, drag at the bed, is small in the thick ice of the upper basin and the very thick ice in the upper basin shows resistance as minimal as 40 kPa while the resistance to flow over the riegel is 210 kPa. Evaluating the importance of each term relative to the driving stress shows that the longitudinal drag (2.7b) increases the driving stress by 50% at the riegel and resists 40% of the driving stress in the overdeepening ($y = 5200$). Side drag is less important (2.7c) except at the riegel ($y = 6400$) where it resists 50% of the driving stress. The stress-gradient coupling terms together show that only half of the resistance to flow is from basal drag within the overdeepening (2.7d). This is an important result as the terms that are often ignored have a major effect.

2.4. UNCERTAINTIES

Ice thickness: Uncertainties in the ice thickness arise from uncertainty in the wave speed within ice, uncertainty in picking the bed reflector (largely caused by side reflections) and errors in interpolation and extrapolation. At the time of the radar survey snow was 1–4 m thick. Almost all of the survey transects are below the 2008–10 ELA, so firn thickness would be minimal even on the highest radar transect. Where radar transects intersect, the root-mean-square difference between observed thicknesses is 13 m. Uncertainties in the depth estimate also arise from both uncertainties in the wave speed in ice ($2 \text{ m } \mu\text{s}^{-1}$, $\sim 1.2\%$ of the depth of the reflector) and from the ambiguity in picking

travel time to a reflector ($0.03 \mu\text{s}$, $\sim \pm 2.5 \text{ m}$). The resulting uncertainty varies from 14–15 m for the range of measured thicknesses at Eklutna Glacier.

Within the survey network, we use a jack knife method (Tukey 1958) to evaluate the sensitivity of our methods. We removed one of the middle cross-flow transects, repeated our interpolation method, and then calculated the residual between the jack-knifed interpolation and the measured transect. The residuals were small ($< 2\%$), resulting in a total uncertainty in ice thickness that varies from $\pm 15 \text{ m}$ in shallower ice to $\pm 17 \text{ m}$ in the thickest ice. Outside the survey network area we do not attempt to quantify the uncertainty. The errors are likely much larger; however we do not use those data in our analysis.

Flow Field: Uncertainties in stake positions are calculated using loop closure methods. Maximum 1.96σ (95% confidence) horizontal uncertainty in stake position was $\pm 1.8 \times 10^{-2} \text{ m}$.

Uncertainties in velocity are minimized by the length of time elapsed between surveys, and within the survey network maximum 1.96σ uncertainty was $1.1 \times 10^{-3} \text{ m d}^{-1}$, compared to overall velocities of 0.052 to 0.181 m d^{-1} . On the mass balance stakes the uncertainty in velocity is greater (because of the single frequency GPS), but that is partially attenuated by the longer intervals between measurements. The resulting maximum 1.96σ uncertainty in velocity was 0.012 m d^{-1} .

Force Balance: Uncertainties in the force balance arise from measurement accuracy and simplifying assumptions. As we co-located radar transects with the survey network, ice-thickness measurement uncertainty is ≤ 17 m. Uncertainty in surface velocity is $< 2\%$ for the slowest portion of the network and $< 1\%$ in the faster areas. For our particular situation the majority of the uncertainty likely arises from the simplifying assumptions. Equation (5) is only strictly applicable to glaciers where the entire ice velocity at the surface is accommodated by basal sliding, i.e. plug flow. The effect of this assumption is that it overestimates the depth-averaged velocity in glaciers with significant internal shear. Most previous applications of the van der Veen (1999) style force balance either explicitly show that most of the ice velocity at the surface is accommodated by basal sliding (O'Neel and others, 2005), or argue that cold ice near the surface acts as a "stress guide" (van der Veen and Whillans 1993; Price and others, 2002), or use an iterative method to estimate forces at different depths (van der Veen and Whillans, 1989b; Kavanaugh and Cuffey, 2009). The dramatic change in cross-sectional area through the reach of interest on the main branch of Eklutna Glacier (from 4.43×10^5 m² to 1.5×10^5 m² in a horizontal distance of 1355 m) makes it difficult to apply similar reasoning. Instead, we made an estimate of the depth averaged velocities with continuity constraints. This makes it challenging to accurately assess our uncertainties as we don't know how good the estimate of ϕ is.

The spacing of the survey network is $1.2\text{--}2.2 H$, so the corresponding force balance is calculated over $2.4\text{--}4.4 H$. This spatial resolution avoids the non-linear error

propagation inherent in the ill-posed boundary value problem of inferring basal conditions purely from surface observations (e.g., Bahr and others, 1994).

Overall we hesitate to interpret all of the details of the force balance. However, the larger patterns are reasonable estimates.

2.5. DISCUSSION

The enhanced thinning in the upper basin is presently impacting the surface mass balance. The accumulation zone is relatively flat and that thinning results in both a downward shift in the area altitude distribution, and an increase in flux out of the upper basin which supports an extended terminus position. Many of the basic assumptions about how mountain glaciers behave, particularly in response to changes in climate, are deeply rooted in simplifications that ignore the “higher-order” terms that arise from stress-gradient coupling of ice (e.g., Nye, 1960; Fowler and Larsen 1978; Hutter, 1981). However, at Eklutna Glacier accounting for these stress-gradient terms are a critical component of understanding the present ice flow out of the upper basin. Our discussion focuses on the overarching question of why the stress-gradient coupling terms are important at this glacier and then considers potential implications if this situation is more common than is often assumed.

Both the radar data and the flow-field indicate that the bed geometry inhibits ice flow out of the upper basin by forcing high rates of vertical compression, resulting in a near tripling of the surface velocities in ~ 2 km distance.

2.5.1. Geometric control of the flow-field

Resolving the bed geometry provides insights into the surface velocities. Convergence above the riegel is both vertical and lateral. Within the previously mentioned constricting reach the maximum constriction occurs with a 48% reduction in area over 630 m, < 2 local ice thicknesses. At the thickest ice ($y = 4900$), the cross-sectional area is $4.4 \times 10^5 \text{ m}^2$. At the riegel ($y = 6400$) the cross sectional area is $1.5 \times 10^5 \text{ m}^2$, a 65% reduction over a horizontal distance of 1355 m. A 48% reduction in cross sectional area occurs in the middle 630 m, i.e., the cross-sectional area is nearly halved over a horizontal distance that is less than 2x the average centerline ice thickness along that distance. The incompressibility condition requires the increase in velocities as the cross-sectional area diminishes. The section of maximum constriction is coincident with the transition from inefficient flow, where the depth averaged velocity is less than 0.8 of the surface velocity, to efficient flow, where the depth averaged velocity \approx surface velocity.

2.5.2. Force balance

There are two unusual aspects about the force balance terms (Figure 2.7). The first is the positive value of longitudinal drag (τ_L) coincident with the overdeepening, from $y = 4500$ to $y = 6000$. Ice flow, as we have noted previously, accelerates through the constricting reach. In many cases along flow accelerations are caused by increases in both surface and bed slope. The resulting tensile longitudinal stress pulls the column of ice forward and effectively adds to the driving stress where the driving stress is low

(Cuffey and Patterson, 2010). This serves to accelerate the ice as it approaches the steeper section of the bed, effectively smoothing the along-glacier velocity fluctuation. Within the constricting reach, the along-flow acceleration is forced by the reduction in cross sectional. Not only do the valley walls come together, the bed rises up. In this case it is no surprise that τ_L has the effect of restraining the flow despite the along-flow acceleration. In other words τ_L is accentuating the variation in driving stress rather than buffering it in order to overcome the changes in cross-sectional area. The geometric control provided by the constricting reach is the governing factor in the pattern of flow, and the change in surface slope is of secondary importance.

The second aspect is that the combination of longitudinal drag, τ_L , and side-wall drag, τ_W , is approximately equal to drag at the bed, τ_b , near the maximum overdeepening. The combination of the longitudinal and side-wall drags can be referred to as stress-gradient coupling, and together they smooth out spatial variability in surface velocities. At the riegel ($y = 6400$) those terms cancel each other out, so the effects are not evenly distributed, but in the upper basin, where the ice is presently thinning, these terms support half of the driving stress despite the fact that the glacier is basically broad and flat.

2.5.3. Implications

The present ice surface elevations in the upper basin are supported in significant part by the combined stress-gradient coupling terms. This is the same are that exhibits

enhanced thinning. It seems likely that the stress-gradient coupling terms are responsible for this pattern and that it will continue into the future. This has implications for the water resources from Eklutna Glacier. The upper basin is still storing a large quantity of ice, however, eventually the flux will have to decrease, at which point the terminus will retreat dramatically and the runoff will be reduced. While the basal geometry at Eklutna Glacier is dramatic, there is no reason to think Eklutna Glacier is one of a kind. If the stress gradient coupling terms are important on other glaciers it could have implications for climate response and water resources there as well, where for some amount of time negative mass balance is maintained in part by enhanced flux delivery to the lower glacier.

2.6. CONCLUSIONS

We documented a significant overdeepening under the broad upper basin, with ice thickness up to 430 ± 17 m. The constriction down glacier is underlain by a bedrock riegel, with ice thicknesses of 260 ± 16 m. The corresponding change in cross-sectional area is from $4.4 \times 10^5 \text{ m}^2$ to $1.5 \times 10^5 \text{ m}^2$, a 65% reduction over a horizontal distance of 1355 m. The pattern of surface velocities within the survey network is largely governed by the geometry, maximum velocities of $66.1 \pm 0.2 \text{ m a}^{-1}$ are above the riegel, minimum velocities of $18.9 \pm 0.2 \text{ m a}^{-1}$ are in the expanding reach upstream of the overdeepening. The force balance results show that the longitudinal drag is in phase with the driving stress instead of the more common out of phase relationship. This shows that

longitudinal drag is largely acting to buffer the changes in ice thickness and cross sectional area rather than the variation in driving stress. The combination of longitudinal and side-wall drag, i.e. the terms that dynamically couple faster and slower flow, resist half of the driving stress in the thickest ice of the upper basin. These stress-gradient coupling terms are sometimes called "higher order" terms and are often ignored. At Eklutna Glacier the present pattern of ice-flux and hence the present mass balance is largely controlled by these terms. It seems likely that this is the case on many mountain glaciers, that we have just overlooked it previously.

Acknowledgements

Special thanks to John Sykes, to all the students of Alaska Pacific University annual glaciology field courses, and to everyone else who helped with fieldwork. Thanks to NASA for an Earth and Space Science Fellowship, Anchorage Municipal Light and Power and Jim Posey for funding most of the fieldwork, and the NIWR for funding many of my field assistants. Thanks to Doug MacAyeal for discussion of the forcing mechanism.

References

- Bahr, D.B., W.T. Pfeffer, M.F. Meier. 1994. Theoretical limitations to englacial velocity calculations. *J. Glaciol.*, **40**(136), 509-518.
- Brown, C.S., M.F. Meier, and A. Post. 1982. Calving speed of Alaska tidewater glaciers, with application to Columbia Glacier. *USGS Prof. Paper*, 1258-C.
- Böðvarsson, G. 1955. On the flow of ice-sheets and glaciers. *Jökull.*, **5**, 1-8.
- Cook, R.D., D.S. Malkus, M.E. Plesha, R.J. Witt. 2002. *Concepts and applications of finite element analysis*. Fourth Ed. John Wiley and Sons. New York, NY.
- Cuffey, K.M., and W.S.B. Patterson. 2010. *The physics of glaciers*, 4th ed. Oxford, etc. Elsevier
- Farinotti, D., M. Huss, A. Bauder, M. Funk, and M. Truffer. 2009. A method to estimate the ice volume and ice-thickness distribution of alpine glaciers. *J. Glaciol.*, **55**(191), 422-430.
- Fowler, A.C., D. A. Larson. 1978. On the flow of Polythermal Glaciers. I. Model and Preliminary Analysis. *Proc. Of the Royal Soc. London. Series A, Math and Physical Sciences*, **363**(1713), 217-242.
- Glen, J.W. 1952. Experiments on the deformation of ice. *J. Glaciol.*, **2**(12), 111-114.
- Harrison, W.D., D.H. Elsberg, K.A. Echelmeyer, and R.M. Krimmel. 2001. On the characterization of glacier response by a single time-scale. *J. Glaciol.*, **47**(159), 659-664.
- Hutter, K. 1981. The effect of longitudinal strain on the shear stress of an ice sheet: in defence of using stretched coordinates. *J. Glaciol.*, **27**(95), 39-56.
- Johannesson, T., C. Raymond, and E. Waddington. 1989. Time-scale for adjustment of glaciers to changes in mass balance. *J. Glaciol.*, **35**(121), 355-369.
- Kamb, B. and K.A. Echelmeyer. 1986. Stress-gradient coupling in glacier flow: 1. Longitudinal averaging of the influence of ice thickness and surface slope. *J. Glaciol.*, **32**(111), 267-284.
- Kamb, B., and 7 others. 1985. Glacier surge mechanism: 1982-1983 surge of Variegated Glacier, Alaska. *Science*. **227**(4686), 469-479.

- Kavanaugh, J.L., K.M. Cuffey, D.L. Morse, H. Conway, E. Rignot. 2009. Dynamics and mass balance of Taylor Glacier, Antarctica: 1. Geometry and surface velocities. *J. Geophysical Research*. 114. F04010
- Kavanaugh, J.L., and K.M. Cuffey. 2009. Dynamics and mass balance of Taylor Glacier, Antarctica: 2. Force balance and longitudinal coupling. *J. Geophysical Research*. 114. F04011
- Meier, M.F., and A. Post. 1987. Fast tidewater glaciers. *J. Geophys. Res.* **92**(B9), 9051-9058.
- Nye, J.F. 1952. The mechanics of Glacier flow. 1952. *J. Glaciol.*, **2**(12). 82-93.
- Nye, J.F. 1957. *Physical Properties of Crystals: Their Representation by Tensors and Matrices*. Oxford University Press
- Nye, J.F. 1960. The response of glaciers and ice-sheets to seasonal and climatic changes. *Proceedings of the Royal Society of London*, **256**(1287), 559-584.
- O'Neel, S., W.T. Pfeffer, R. Krimmel, M. Meier. 2005. Evolving force balance at Columbia Glacier, Alaska, during its rapid retreat. *J. Geophysical Research*. 110. F03012.
- Oerlemans, J., and 8 others. 2005. Estimating the contribution of Arctic glaciers to sea-level change in the next 100 years. *Annals of Glac.* **42**, 230-236.
- Pfeffer, W. T. 2007. A simple mechanism for irreversible tidewater glacier retreat. *Journal of Geophysical Research—Earth Surface*. **112** (F3): F03S25.
- Price, S.F., R.A. Bindshadler, C.L. Hulbe, D.D. Blankenship. 2002. Force balance along and inland tributary and onset to Ice Stream D, West Antarctica. *J. Glaciol.*, **48**(160). 20-30.
- Sass, L.C., M.G. Loso, S.O'Neel, C.F. Larsen. In Prep. Characterizing surface mass balance and geometry change at Ekltuna Glacier, Alaska. *J. Glaciol.*, XX(XXX). XX-XX
- Seroussi, H., M. Morlighem, E. Rignot, E. Larour, D. Aubrey, H. Ben Dhia, and S.S. Kristensen. 2011. Ice flux divergence anomalies on 79north Glacier, Greenland. *Geophysical Research Letters*, **38** L09501
- Sibson, R. 1981. A brief description of natural neighbor interpolation. In *Interpreting multivariate data*. V. Barney, ed. John Wiley and Sons, Chinchester. 21-36.
- Tukey, J.W. 1958. Bias and confidence in not-quite large samples. *The Annals of Mathematical Statistics*. **29** (2) 614-

- van der Veen, C.J. 1999. *Fundamentals of glacier dynamics*. A.A. Balkema, Rotterdam
- van der Veen, C.J., and Whillans, I.M. 1989. Force budget: 1. Theory and numerical methods. *J. Glaciol.*, **35**(119). 53-60.
- van der Veen, C.J., and Whillans, I.M. 1989. Force budget: 2. Application to two-dimensional flow along Byrd Strain Network, Antarctica. *J. Glaciol.*, **35**(119). 61-67.
- van der Veen, C.J., and Whillans, I.M. 1993. Location of mechanical controls on Columbia Glacier, Alaska, U.S.A., prior to its rapid retreat. *J. Glaciol.*, **35**(119). 53-60.

Appendix 2.1. Table of surface velocities

pole	Easting	Northing	elevation	$u \text{ m a}^{-1}$	1.96σ
1	394002.70	6790703.03	1242.97	46.76	0.13
2	393750.33	6790649.60	1845.95	65.33	0.41
3	393492.79	6790587.12	1243.07	57.44	0.13
4	394075.25	6790410.39	1264.79	56.90	0.13
5	393832.15	6790344.56	1265.17	64.54	0.13
6	393564.24	6790270.69	1892.28	57.03	0.41
7	394171.33	6790145.08	1301.96	55.05	0.13
8	393957.96	6790045.71	1303.12	66.12	0.13
9	393709.79	6789948.45	1303.55	61.51	0.13
10	394296.32	6789897.09	1324.04	50.23	0.13
11	394085.66	6789781.69	1326.64	56.25	0.13
12	393874.29	6789664.28	1325.14	50.88	0.13
13	394435.58	6789674.59	1343.45	44.17	0.13
14	394223.04	6789539.46	1341.70	48.60	0.13
15	394011.72	6789422.55	1339.13	45.15	0.13
16	394687.93	6789398.33	1360.81	36.59	0.13
17	394413.64	6789240.28	1985.90	41.28	0.41
18	394128.91	6789113.70	1357.42	38.16	0.13
19	395006.71	6789039.00	1377.11	29.30	0.13
20	394573.18	6788837.92	1368.46	34.23	0.13
21	394162.78	6788701.33	1380.08	29.79	0.13
22	395226.00	6788565.44	1384.54	26.58	0.13
23	394701.12	6788415.75	1382.31	31.13	0.13
24	394219.74	6788287.67	1392.30	26.62	0.13
25	395458.54	6788008.18	1405.24	23.78	0.13
26	394849.25	6787854.47	1398.49	28.54	0.13
27	394237.07	6787706.69	1404.82	21.71	0.13
28	395746.70	6787314.61	1432.29	18.88	0.13
29	394997.43	6787158.12	1428.29	28.64	0.13
30	394237.33	6787072.25	1430.34	23.06	0.13

Data CD contents

The data CD contains four folders, for mass balance, surface elevations, radar data, and GPS data. Each folder contains the raw or nearly raw data, the matlab codes and functions used to manipulate the data, and a read me text file that explains the contents of the folder.